

PUBLISHED VERSION

D. Hasterok, J. Webb

On the radiogenic heat production of igneous rocks

Geoscience Frontiers, 2017; 8(5):919-940


© 2017, China University of Geosciences (Beijing) and Peking University. Production and hosting by Elsevier B.V. This is an open access article under the CC BY-NC-ND license (<http://creativecommons.org/licenses/by-nc-nd/4.0/>).

Originally published at:

<http://doi.org/10.1016/j.gsf.2017.03.006>

PERMISSIONS

<http://creativecommons.org/licenses/by-nc-nd/4.0/>



**Attribution-NonCommercial-NoDerivatives 4.0 International
(CC BY-NC-ND 4.0)**


This is a human-readable summary of (and not a substitute for) the [license](#). [Disclaimer](#).


You are free to:


Share — copy and redistribute the material in any medium or format

The licensor cannot revoke these freedoms as long as you follow the [license terms](#).

Under the following terms:

 **Attribution** — You must give [appropriate credit](#), provide a link to the license, and [indicate if changes were made](#). You may do so in any reasonable manner, but not in any way that suggests the licensor endorses you or your use.

 **NonCommercial** — You may not use the material for [commercial purposes](#).

 **NoDerivatives** — If you [remix, transform, or build upon](#) the material, you may not distribute the modified material.

No additional restrictions — You may not apply legal terms or [technological measures](#) that legally restrict others from doing anything the license permits.

21 September 2017

<http://hdl.handle.net/2440/107235>

HOSTED BY



ELSEVIER

Contents lists available at ScienceDirect

China University of Geosciences (Beijing)

Geoscience Frontiers

journal homepage: www.elsevier.com/locate/gsf

Research paper

On the radiogenic heat production of igneous rocks

D. Hasterok^{a,*}, J. Webb^{a,b}^a Department of Earth Sciences, University of Adelaide, North Terrace, SA, 5005, Australia^b Ramelius Resources Ltd., East Perth, WA, 6005, Australia

ARTICLE INFO

Article history:

Received 30 November 2016

Received in revised form

18 March 2017

Accepted 21 March 2017

Available online 4 May 2017

Handling Editor: M. Santosh

Keywords:

Heat generation

Igneous rocks

Heat producing elements

Continental lithosphere

Seismic velocity

Density

ABSTRACT

Radiogenic heat production is a physical parameter crucial to properly estimating lithospheric temperatures and properly understanding processes related to the thermal evolution of the Earth. Yet heat production is, in general, poorly constrained by direct observation because the key radiogenic elements exist in trace amounts making them difficult to image geophysically. In this study, we advance our knowledge of heat production throughout the lithosphere by analyzing chemical analyses of 108,103 igneous rocks provided by a number of geochemical databases. We produce global estimates of the average and natural range for igneous rocks using common chemical classification systems. Heat production increases as a function of increasing felsic and alkali content with similar values for analogous plutonic and volcanic rocks. The logarithm of median heat production is negatively correlated ($r^2 = 0.98$) to compositionally-based estimates of seismic velocities between 6.0 and 7.4 km s⁻¹, consistent with the vast majority of igneous rock compositions. Compositional variations for continent-wide models are also well-described by a log-linear correlation between heat production and seismic velocity. However, there are differences between the log-linear models for North America and Australia, that are consistent with interpretations from previous studies that suggest above average heat production across much of Australia. Similar log-linear models also perform well within individual geological provinces with ~1000 samples. This correlation raises the prospect that this empirical method can be used to estimate average heat production and natural variance both laterally and vertically throughout the lithosphere. This correlative relationship occurs despite a direct causal relationship between these two parameters but probably arises from the process of differentiation through melting and crystallization.

© 2017, China University of Geosciences (Beijing) and Peking University. Production and hosting by Elsevier B.V. This is an open access article under the CC BY-NC-ND license (<http://creativecommons.org/licenses/by-nc-nd/4.0/>).

1. Introduction

Radiogenic heat production affects lithospheric temperatures, thereby influencing many physical property magnitudes and processes operating within the solid Earth. In extreme cases, the distribution of heat producing elements facilitates high-temperature regional metamorphism (McLaren et al., 1999; Kramers et al., 2001; Kelsey and Hand, 2015), internal deformation (Sandiford et al., 2001), and dramatically affects the thickness of the lithosphere (Artemieva and Mooney, 2001; Hasterok and Chapman, 2011). However, the distribution of heat producing elements (HPEs) that internally heat the lithosphere is poorly constrained (Hasterok and

Chapman, 2011; Jaupart et al., 2016). Most thermal and geodynamic models incorporate very rudimentary models of heat production, often assuming an exponential decrease or constant layered values with depth (e.g., McKenzie et al., 2005; Artemieva, 2006; Hasterok and Gard, 2016). Allowable variations in heat production can lead to profound differences in physical behavior as deep lithospheric temperatures are highly sensitive to shallow variations in heat production (Sandiford et al., 2001; Hasterok and Chapman, 2011), and yet these uncertainties are rarely propagated through thermal and geodynamic models.

In some instances, vertical variations in lithospheric heat production are improved by radiometric profiles along upturned and exposed crustal cross-sections (e.g., McLaren et al., 2003; Brady et al., 2006; Roy et al., 2008). Besides being rare, exposed cross-sections have limited utility because they rarely project to conditions below the upper crust and may not approximate the average crust (Hasterok and Chapman, 2011). Xenoliths, while also

* Corresponding author.

E-mail address: dhasterok@gmail.com (D. Hasterok).

Peer-review under responsibility of China University of Geosciences (Beijing).

rare, are problematic as they may not adequately sample the entire lithosphere and can interact with magmatic fluids during ascent, increasing the concentration of heat producing elements above in situ values (Dawson, 1984). Surface heat flow, thermal isostatic, and seismic estimates of mantle temperatures provide constraints on total heat production, but poorly constrain their vertical distribution (e.g., Goes and van der Lee, 2002; Jaupart and Mareschal, 2003; Hasterok and Gard, 2016).

Our aim in this study is two-fold: to determine the global average and natural variability of heat production for igneous rocks as a function of chemistry; and to seek a means by which heat production may be estimated vertically through the lithosphere.

Through examination of heat production as a function of chemistry, we find a systematic increase in the global average heat production from ultramafic to mafic to felsic rocks. Using this correlation, we revisit the possibility of an empirical relationship between heat production and geophysical properties, specifically density and seismic velocity first suggested by Rybach (1973, 1978/79). Such a relationship can be used in future studies to produce more reliable estimate lateral and vertical heat production—and its uncertainty—throughout the lithosphere in poorly characterized regions.

2. Methods

We compute three physical properties from major and trace element chemistry in this study: heat production, density, and seismic velocity. Advances in thermodynamic modeling permit the use of chemical and/or mineralogical data to estimate density and seismic velocity (Behn and Kelemen, 2003; Abers and Hacker, 2016). There are limitations to this approach (Section 5.5), but it allows us to utilize vast quantities of readily available geochemical data.

Despite limitations, the accuracy of thermodynamic modeling is sufficient that they are widely used to model mineral assemblages, physical properties and physical processes across a number of geoscientific subdisciplines. For example, thermodynamic models are routinely used to model rock phases (including solid solutions) to develop pressure–temperature–time paths of real rocks (e.g. Kelsey et al., 2008; Kelsey and Hand, 2015). Sophisticated thermodynamic codes such as PerpleX (Connolly, 1990) have been in use for over a decade to estimate physical properties necessary to model geodynamic processes (e.g., Hacker et al., 2003; Stixrude and Lithgow-Bertelloni, 2005; Afonso et al., 2008; Zunino et al., 2011; Brown, 2014). The resulting geodynamic models generally provide sufficiently accurate simulations of the Earth's evolution to model match observations of physical parameters such as gravity (based on density) and seismic velocity (e.g., Gerya et al., 2001; Behn and Kelemen, 2003; Afonso et al., 2008).

2.1. Heat production, A

Heat production is determined from the chemical composition with the relationship

$$A(\mu\text{Wm}^{-3}) = \rho(9.67C_U + 2.56C_{Th} + 2.89C_{K_2O}) \times 10^{-5} \quad (1)$$

with concentrations, C , of HPEs in parts per million (ppm) except K_2O in weight percent (wt.%), and density, ρ , in kg m^{-3} (Rybach, 1988).

2.2. Seismic velocity, V_p

To estimate seismic velocity we use an empirical model developed by Behn and Kelemen (2003). Their model is calibrated to

>18,000 igneous rocks in the IGBA database, which encompasses a range of compositions (Brandle and Nagy, 1995). The igneous rock compositions were equilibrated to 800 °C and a range of pressures <2 GPa using PerpleX (Connolly, 1990). Calculated mineral assemblages were then used to estimate density and elastic moduli with mineral physical properties compiled by Sobolev and Babeyko (1994) and Bass (1995). These moduli were then used to estimate bulk seismic velocity averaging individual mineral components using the Hashin-Shtrickman bounds (Berryman, 1995). Behn and Kelemen (2003) then extended these computations to a greater range of temperatures and pressures for a depth range from 5 to 50 km along an average geothermal gradient (Chapman and Pollack, 1977).

The thermodynamic calculations by Behn and Kelemen (2003) were validated by comparison to 139 high quality laboratory measurements. Good agreement was found with a 1:1 line (Fig. 5 of Behn and Kelemen, 2003). The thermodynamic calculations predict systematically higher values than laboratory estimates for seismic velocity ($0.05 \pm 0.12 \text{ km s}^{-1}$, <1% average error). However, this error is relatively small compared to typical uncertainties estimated from field studies.

With the thermodynamic calculations validated, Behn and Kelemen (2003) developed several empirical models with which to estimate seismic velocity from selected oxides. To compute seismic velocity in this study, we use the compositional model

$$V_P(\text{km/s}) = 6.9 - 0.011C_{\text{SiO}_2} + 0.037C_{\text{MgO}} + 0.045C_{\text{CaO}} \quad (2)$$

where the concentration of each oxide is in weight percent. An advantage of this technique is that it requires just three major oxide concentrations to compute seismic velocity. Estimated uncertainty in seismic velocity is $\pm 0.13 \text{ km s}^{-1}$ (1σ) using this approach. While a more complete suite of oxides can be used to estimate seismic velocity with an uncertainty of $\pm 0.12 \text{ km s}^{-1}$, there is no significant improvement in velocity uncertainty over the three oxide method (Behn and Kelemen, 2003). A drawback of this method is that it is calibrated for anhydrous compositions only, the implications of which are addressed in Section 5.5.1.

Table 1
Coefficients for multilinear density models.

Component	Coefficient	($-\alpha_{95}$, α_{95})
<i>Model 1</i>		
ρ_0	60,425.0	(50,595.4/70,254.5)
SiO ₂	−600.2	(−698.2/−502.1)
Al ₂ O ₃	−373.6	(−485.8/−261.4)
MgO	−564.9	(−663.2/−466.5)
FeO	−474.3	(−575.9/−372.6)
CaO	−663.1	(−762.5/−563.7)
Na ₂ O	−1497.9	(−1726.8/−1268.9)
K ₂ O	51.9	(−129.3/233.1)
<i>Model 2</i>		
ρ_0	3111.5	(3103.8/3119.1)
SiO ₂	−4.6	(−4.7/−4.5)
MgO	8.5	(8.3/8.7)
CaO	5.7	(5.4/6.0)
<i>Model 3</i>		
ρ_0	4770.5	(4754.1/4786.8)
SiO ₂	−23.2	(−23.4/−23.0)
Al ₂ O ₃	−23.4	(−23.7/−23.1)
MgO	−7.6	(−7.8/−7.4)
Na ₂ O	−12.8	(−13.5/−12.0)
<i>Model 4</i>		
ρ_0	2606.7	(2602.5/2610.5)
Fe*	174.7	(170.5/178.9)
MALI	−12.0	(−12.2/−11.8)
ASI	49.6	(47.2/52.0)
Maficity	636.0	(630.1/642.0)

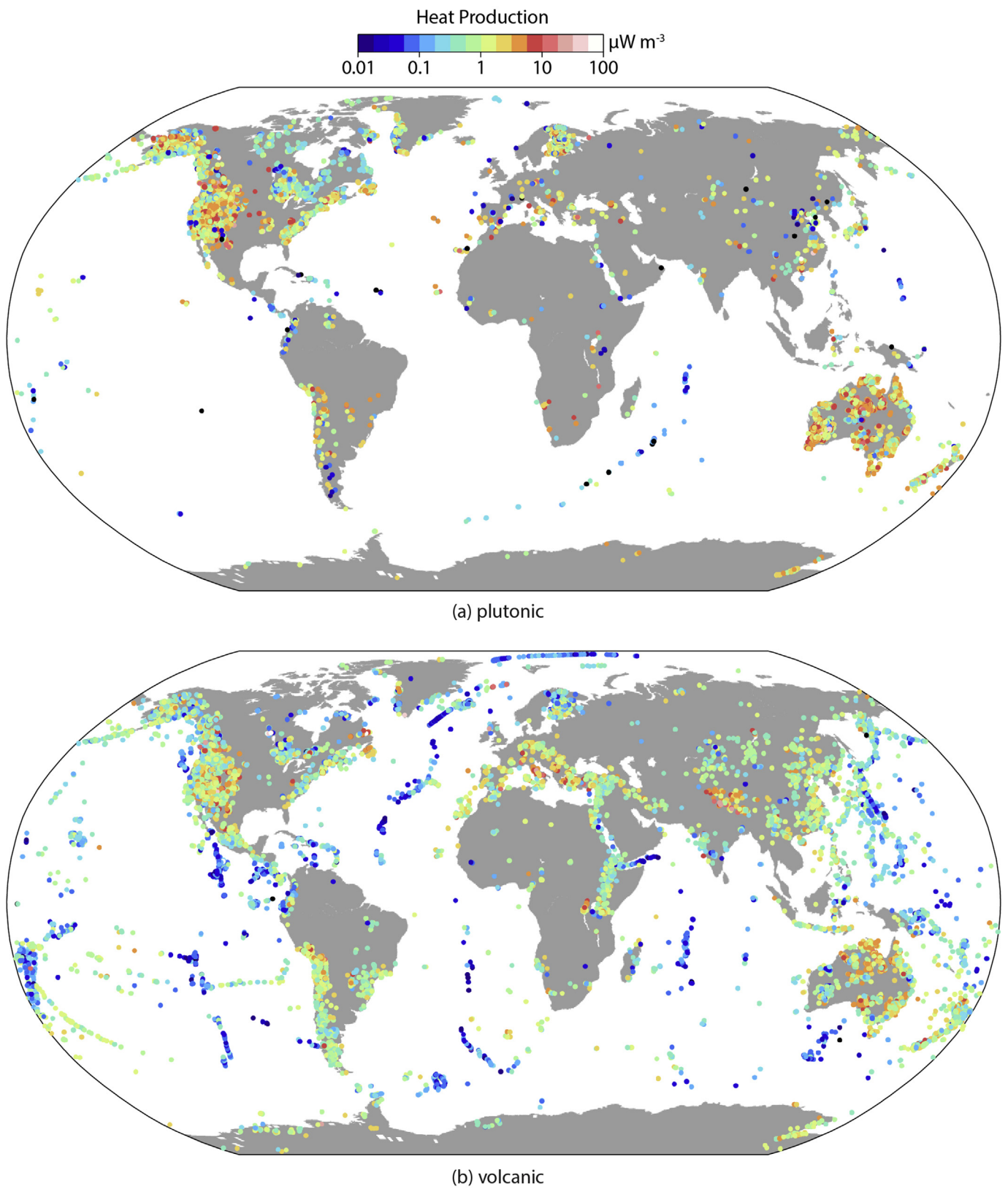


Figure 1. Locations of (a) plutonic and (b) volcanic rocks with chemistry sufficient for P-wave and heat production estimates. Estimates of heat production determined from Equation (1).

2.3. Density, ρ

Behn and Kelemen (2003) did not develop a density model from oxide weight percentages, but density was computed as part of their analysis. To ensure self-consistency we use the results of their thermodynamic calculations (M. Behn, pers. comm.) to produce a multiple linear regression model to estimate density. We tested several formulations including the four listed below:

- (1) seven oxides (SiO_2 , Al_2O_3 , MgO , FeO^T , CaO , Na_2O , and K_2O);
- (2) SiO_2 , MgO and CaO (same oxides as Behn and Kelemen (2003) preferred model for V_p);
- (3) SiO_2 , Al_2O_3 , MgO , Na_2O ;
- (4) geochemical indices (Fe-number, MALI, ASI, and maficity as defined below).

Regression coefficients for the four models are given in Table 1.

Model 1 and 3 work best with an average error of $\sim 2\%$ (Fig. 2). Model 4 has an average error of $\sim 3\%$, while model 2 has the highest error ($\sim 4\%$). However, because of the wider range of compositions in the geochemical databases relative to the calibration study, model 1 produces the worst result in practice, resulting in numerous and unrealistic outlying values (e.g., <0 or $>4000 \text{ kg m}^{-3}$). Model 2 produces the fewest outliers, perhaps because the range of these elements is generally large and is captured by the calibrated compositions. Models 3 and 4 are generally well behaved, but do produce some outliers. Most estimates lie within the typical bounds reported for plutonic rocks (Telford et al., 1990).

The PETROCH database (Haus and Pauk, 2010) includes estimates of density which we can use to further validate and choose the appropriate model. Model 4 performs the best in this regard (Fig. 3); however, this model is systematically higher than the PETROCH data by approximately 120 kg m^{-3} (4 to 5%). Behn and

Kelemen (2003) also observed a systematic overprediction of density compared with laboratory data, which could be due to porosity/cracks in the natural samples or hydrous phases excluded from the thermodynamic models. Model 4, developed from geochemical indices has an additional advantage in that indices may be better behaved than any single element.

After correcting for density, our preferred model (Model 4) for estimating density is given by

$$\rho = 2486.5 + 174.7 \text{ Fe}^* - 12.0 \text{ MALI} + 49.6 \text{ ASI} + 636.0 \text{ maficity} \quad (3)$$

where the geochemical indices are defined as

$$\begin{aligned} \text{Fe}^* (\text{iron number}) &= C_{\text{FeO}^T} (C_{\text{FeO}^T} + C_{\text{MgO}})^{-1} \\ \text{MALI} (\text{modified alkali-lime index}) &= C_{\text{Na}_2\text{O}} + C_{\text{K}_2\text{O}} - C_{\text{CaO}} \\ \text{ASI} (\text{alumina saturation index}) &= n_{\text{Al}} (n_{\text{Ca}} - 1.67n_{\text{p}} + n_{\text{Na}} + n_{\text{K}})^{-1} \\ \text{Maficity} &= n_{\text{Fe}} + n_{\text{Mg}} + n_{\text{Ti}} \end{aligned}$$

where n is the number of moles of each specified oxide component and FeO^T is the total iron.

We exclude density estimates computed below 2400 and above 3600 kg m^{-3} to remove the influence of extreme outliers.

3. Geochemical datasets

Whole-rock geochemical data for igneous rocks obtained from a number of online databases and publications are summarized in Table 2. Although we compiled 526,156 igneous samples, only 108,103 had chemical information sufficient to compute velocity, density and heat production (Table 2). Geographic coverage is predominantly concentrated along active plate boundaries, although there are a number of clusters in intraplate settings, most notably Australia and Canada (Fig. 1). Plutonic data are almost

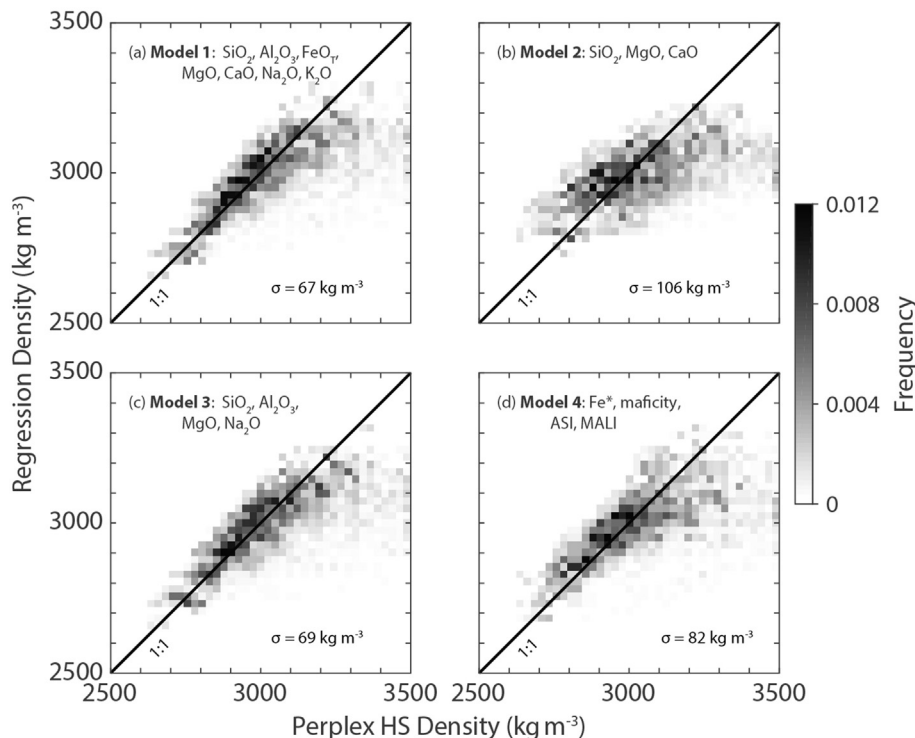


Figure 2. Compositionally-based multiple linear regression models of igneous rock densities. The models are calibrated to thermodynamic calculations performed by Behn and Kelemen (2003) on anhydrous samples with $<25\%$ modal garnet.

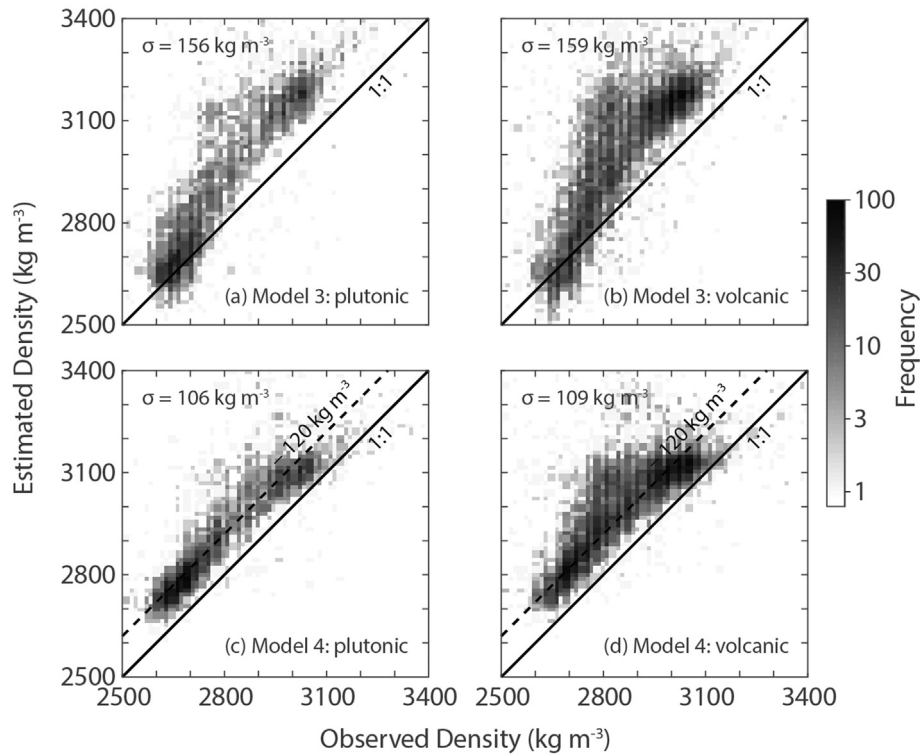


Figure 3. Comparison between PETROCH density data and compositional density estimates from models 3 (a,b) and 4 (c,d). Plutonic data (a,c) and volcanic data (b,d). Solid and dashed lines each have a slope of 1 with the dashed line (c,d) including a reduction of modeled density by 120 kg m^{-3} . σ is the standard deviation of residuals.

entirely constrained to continental regions (Fig. 1a). Volcanic data are largely coincident with plutonic data on the continents with the addition of a large number of oceanic samples (Fig. 1b).

A few corrections/adjustments are made to the database prior to computing physical properties. In some databases, a handful of samples provide some or all major oxides in ppm rather than the labeled weight percent. This is generally easy to identify as the values exceed 100 for a single oxide. These data are converted to weight percent.

Before computing physical properties, the major oxides (SiO_2 , TiO_2 , FeO , MgO , CaO , Na_2O , K_2O , P_2O_5) are normalized to 100% on a volatile-free basis with total iron expressed as FeO . Less common oxides (Cr_2O_3 , NiO , MnO , or BaO) are typically low in abundance (<1 wt.%) and are not commonly reported within the databases. Thus we excluded them in the normalization in order to ensure consistent treatment of all samples.

Table 2

Plutonic and volcanic samples with velocity, density and heat production estimates.

Database	Plutonic N_p	Volcanic N_p	Reference ^a
EarthChem	18,396	58,649	EarthChem.org
OzChem	11,213	5670	Champion et al. (2016)
Canada	5918	1056	Various ^b
GNS PETLAB	2042	1752	Strong et al. (2016)
RGDB	2754	493	Rasilainen et al. (2007)
Ujarassiorit	135	25	Geological Survey of Greenland (2011)
Total	40,458	67,645	

^a See [Supplementary Material](#) for list of individual references within various databases.

^b BC Geochemical database, Lett and Ronning (2005); PETROCH, Haus and Pauk (2010); GSC Open Files, Ernst and Buchan (2010) and Whalen et al. (2012); Geo-Atlas, Newfoundland and Labrador Geological Survey (2009b) and Newfoundland and Labrador Geological Survey (2009a).

The EarthChem database includes a hierarchical rock naming scheme that other databases used in this study lack. We implement this hierarchical naming scheme as a means to easily filter the dataset. Samples are identified as igneous, metamorphic, sedimentary, or xenolith. We reappportion xenolith data into the other three rock classes based on the given rock name. This adjustment is most important for ultramafic compositions, peridotites and pyroxenites, since other compositions are too few in number relative to their eruptive or intrusive counterparts to skew the results presented here.

Igneous rocks within the EarthChem database are further classified as plutonic or volcanic and are given a name based on a user selected method: assigned by author, TAS classification, or from EarthChem native categories. Author assigned names can be problematic as rock names can be assigned by one of several different classification schemes. For example, modal or normative mineralogy (e.g., QAPF classification), bulk chemistry (e.g., TAS classification), and bulk + trace chemistry are all common methods to assign a rock type (Philpotts and Ague, 2009). While often similar, there is not perfect correspondence between schemes. Furthermore, rock names are often given modifiers based on texture. The additional modifiers to names (e.g., vesicular basalt, rapakivi granite) make it difficult to easily select rocks based on a simple type. Since the method of naming is not listed, it makes it unclear how these names are assigned. In addition, many reported rock names in the chemical databases are wildly different than their chemistry would suggest (e.g., a handful of samples identified as basalt with $\text{SiO}_2 > 65 \text{ wt.}\%$).

To ensure consistency and solve these issues, we choose to use a customized naming scheme based on major element composition in order to ensure consistency across multiple databases, while keeping the hierarchical structure (igneous, plutonic, etc.). There are many chemical classifications of igneous rocks, each with their

own advantages and disadvantages. In this study, we focus on two that are commonly used because of their simplicity and widespread use: the total alkali + silica (TAS) (Middlemost, 1994) and a simplified SIA-type classification schemes (Frost et al., 2001).

An advantage of the TAS classification is a consistent and simple approach to naming samples and which allows for the direct chemical comparison of plutonic and igneous rocks. For high-magnesian volcanics, we include additional classification constraints (i.e., picrite, komatiite, meimechite, and boninite from Le Bas and Streckeisen, 1991). For plutonic rocks with ultramafic compositions, we attempt to separate crustal-derived cumulate rocks from mantle-derived rocks by assuming the majority of mantle-derived rocks have a high Mg#, >0.8 (e.g., Griffin et al., 1999). This distinction between mantle and cumulate forms is important as they have distinctly different physical properties, i.e.,

density and seismic velocity. The number of rocks in each compositional field are found in Tables 3 and 4. Felsic subalkaline rocks are the most commonly sampled plutonic rocks and subalkaline mafic rocks are the most commonly sampled volcanics.

We use a simplified version of the SIA classification scheme (Frost et al., 2001): A-type is defined as ferroan composition, identified by Fe-number (Fe^*) > 0.446 + 0.0046 C_{SiO_2} , S-type with alumina-saturation index (ASI) > 1, and I-type with ASI < 1. The SIA scheme was originally developed in an attempt to separate granitoids with sediment protoliths (S-type) from those with igneous protoliths (I-type) (Chappell and White, 1992). A classification of anorogenic (A-type) was added later (Collins et al., 1992). More recently, these interpretations have been called into question (Bonin, 2007, and references therein), but are still in widespread use and do exhibit chemical variations typical of certain settings,

Table 3

Estimated density and seismic velocity determined for (a) plutonic rocks and (b) volcanic rocks.

TAS field	Rock type	N	P-wave velocity					Density				
			Quantiles (km s^{-1})					Quantiles (kg m^{-3})				
			Q _{0.05}	Q _{0.25}	Q _{0.50}	Q _{0.75}	Q _{0.95}	Q _{0.05}	Q _{0.25}	Q _{0.50}	Q _{0.75}	Q _{0.95}
(a) Plutonic rocks												
A	Quartzolite	58	5.87	5.92	5.97	6.00	6.12	2569	2668	2711	2776	2927
B	Granite	17,827	6.06	6.11	6.15	6.21	6.27	2570	2609	2625	2645	2680
C	Granodiorite	5560	6.28	6.33	6.39	6.46	6.55	2653	2684	2707	2732	2771
D	Diorite	2556	6.50	6.58	6.64	6.72	6.83	2732	2762	2784	2811	2865
E	Gabbroic diorite	2610	6.74	6.84	6.93	7.05	7.27	2825	2861	2898	2937	2996
F	Subalkalic gabbro	2741	6.91	7.04	7.15	7.34	7.87	2904	2949	2977	3013	3255
G	Peridotgabbro	386	7.19	7.41	7.75	8.02	8.19	2998	3074	3170	3322	3413
H ₁	Cumulate peridotite	99	7.15	7.41	7.59	7.88	8.36	3082	3128	3169	3249	3352
H ₂	Mantle peridotite	19	7.92	8.11	8.21	8.27	8.45	3190	3317	3346	3401	3544
I	Quartz monzonite	2429	6.20	6.28	6.34	6.41	6.49	2569	2634	2664	2688	2720
J	Syenite	698	6.20	6.26	6.32	6.40	6.52	2499	2573	2613	2646	2695
K	Monzonite	1497	6.45	6.53	6.60	6.68	6.83	2685	2726	2749	2770	2804
L	Monzodiorite	1083	6.64	6.73	6.8	6.89	7.09	2775	2808	2832	2856	2901
M	Monzogabbro	333	6.81	6.89	6.96	7.17	7.38	2854	2885	2907	2935	2988
N	Alkalic gabbro	851	6.87	6.97	7.04	7.14	7.50	2896	2932	2956	2987	3058
O	Foid monzosyenite	279	6.53	6.63	6.72	6.83	6.91	2650	2699	2723	2748	2784
P	Foid syenite	152	6.26	6.29	6.36	6.46	6.60	2502	2547	2569	2607	2659
Q	Foid monzodiorite	226	6.70	6.88	6.96	7.05	7.20	2731	2764	2801	2830	2878
R	Foid gabbro	404	6.92	7.13	7.43	7.65	7.79	2871	2944	3017	3073	3127
S	Ultra-high alkali plutonic	17	5.98	6.03	6.14	6.24	6.82	2439	2482	2528	2544	2593
T ₁	Intermediate foidolite	18	6.46	6.72	6.88	7.13	7.55	2599	2665	2730	2802	2859
T ₂	Mafic foidolite	28	6.68	7.28	7.46	7.57	7.78	2884	2923	2940	2956	2981
T ₃	Ultramafic foidolite	70	6.59	7.38	7.69	7.88	8.04	2979	3045	3089	3131	3179
(b) Volcanic rocks												
A	Silexite	116	5.83	5.92	5.98	6.01	6.16	2617	2709	2766	2827	3246
B	Rhyolite	10,015	6.05	6.09	6.13	6.20	6.27	2594	2620	2640	2665	2709
C	Dacite	4820	6.27	6.33	6.40	6.48	6.57	2671	2701	2724	2752	2820
D	Andesite	5058	6.51	6.60	6.66	6.74	6.86	2746	2777	2805	2837	2903
E	Basaltic andesite	8646	6.74	6.84	6.92	7.01	7.13	2835	2871	2901	2932	2974
F	Subalkalic basalt	14,192	6.95	7.07	7.14	7.20	7.32	2914	2950	2970	2988	3028
G	Picrobasalt	267	7.04	7.24	7.42	7.53	7.67	3012	3057	3074	3097	3129
I	Trachydacite	2083	6.17	6.26	6.34	6.42	6.50	2605	2647	2677	2702	2727
J	Trachyte	1220	6.20	6.26	6.31	6.38	6.48	2567	2596	2626	2651	2689
K	Trachyandesite	2905	6.45	6.53	6.60	6.68	6.79	2692	2731	2754	2776	2802
L	Basaltic trachyandesite	3529	6.65	6.75	6.82	6.90	7.03	2786	2815	2838	2860	2887
M	Trachybasalt	3488	6.83	6.93	7.00	7.08	7.21	2864	2886	2903	2920	2948
N	Alkalic basalt	6608	6.93	7.04	7.12	7.20	7.35	2903	2938	2962	2986	3022
O	Phonolite	593	6.27	6.30	6.36	6.44	6.52	2537	2559	2585	2614	2639
P	Tephriphonolite	255	6.41	6.55	6.63	6.72	6.85	2647	2673	2698	2731	2767
Q	Phonotephrite	399	6.65	6.80	6.90	6.99	7.17	2753	2786	2812	2834	2863
R	Tephrite	2637	6.94	7.11	7.24	7.37	7.51	2868	2921	2970	3009	3051
S	Ultra-high alkali volcanic	16	5.99	6.13	6.38	6.71	6.81	2462	2518	2574	2612	2653
T ₁	Intermediate foidite	48	6.55	6.66	6.85	7.02	7.43	2600	2674	2751	2821	2856
T ₂	Mafic foidite	46	6.85	7.16	7.19	7.20	7.26	2828	2854	2861	2889	2937
T ₃	Ultramafic foidite	133	7.12	7.41	7.57	7.74	7.94	2979	3025	3056	3087	3146
U	Boninite	8	7.13	7.15	7.20	7.25	7.53	3037	3044	3057	3069	3111
V	Meimechite	20	7.48	7.53	7.72	7.76	7.85	3109	3173	3205	3233	3312
W	Komatiite	78	7.44	7.56	7.64	7.74	7.92	3107	3139	3173	3220	3277
X	Picrite	165	7.41	7.52	7.58	7.66	7.75	3080	3109	3127	3157	3193
Y	Alkali picrite	72	7.28	7.43	7.52	7.63	7.86	3000	3044	3097	3137	3203

Table 4
Heat production of (a) plutonic rocks and (b) volcanic rocks using TAS classification.

TAS field	Rock type	N	Heat production										
			Quantiles ($\mu\text{W m}^{-3}$)					ln \mathcal{N} scale			($\mu\text{W m}^{-3}$)		
			$Q_{0.05}$	$Q_{0.25}$	$Q_{0.50}$	$Q_{0.75}$	$Q_{0.95}$	μ	σ	2 SE	\bar{A}	σ_A	2 SE
(a) Plutonic rocks													
A	Quartzolite	58	0.30	0.73	1.58	2.47	11.33	0.456	1.17	0.155	3.13	28.6	3.79
B	Granite	17,827	0.76	1.77	2.79	4.28	8.18	0.989	0.74	0.006	3.54	9.12	0.070
C	Granodiorite	5560	0.45	0.97	1.53	2.22	3.79	0.361	0.692	0.009	1.82	2.04	0.030
D	Diorite	2556	0.28	0.62	0.94	1.40	2.59	-0.092	0.737	0.015	1.20	1.03	0.020
E	Gabbroic diorite	2610	0.10	0.32	0.49	0.75	1.49	-0.765	0.86	0.017	0.67	0.50	0.010
F	Subalkalic gabbro	2741	0.025	0.12	0.23	0.46	1.23	-1.524	1.231	0.024	0.46	0.77	0.010
G	Peridotgabbro	386	0.003	0.053	0.16	0.40	2.49	-2.022	1.811	0.092	0.68	11.9	0.61
H ₁	Cumulate peridotite	99	0.040	0.093	0.24	1.29	11.80	-0.99	1.737	0.175	1.68	55.0	5.55
H ₂	Mantle peridotite	19	0.006	0.061	0.13	0.37	4.41	-1.799	1.917	0.452	1.04	41.4	9.76
I	Quartz monzonite	2429	0.82	1.52	2.16	3.21	6.70	0.795	0.634	0.013	2.71	3.63	0.070
J	Syenite	698	0.99	1.64	2.58	4.65	9.68	1.027	0.72	0.027	3.62	8.88	0.34
K	Monzonite	1497	0.59	1.05	1.54	2.44	6.34	0.507	0.751	0.019	2.20	3.67	0.090
L	Monzodiorite	1083	0.28	0.64	1.08	1.67	4.52	0.067	0.854	0.026	1.54	2.55	0.080
M	Monzogabbro	333	0.32	0.61	0.95	1.68	4.42	0.076	0.84	0.046	1.53	2.41	0.13
N	Alkalic gabbro	851	0.09	0.26	0.45	0.74	3.52	-0.774	0.999	0.034	0.76	0.99	0.030
O	Foid monzosyenite	279	1.20	2.77	3.43	4.13	6.86	1.224	0.549	0.033	3.95	5.51	0.33
P	Foid syenite	152	1.46	2.19	3.38	6.24	11.37	1.34	0.699	0.057	4.88	15.0	1.22
Q	Foid monzodiorite	226	1.01	2.00	3.42	4.25	9.25	1.135	0.674	0.045	3.90	8.76	0.58
R	Foid gabbro	404	0.24	1.06	2.69	5.73	9.52	0.78	1.262	0.063	4.84	91.6	4.56
S	Ultra-high alkali plutonic	17	1.16	1.71	2.41	5.67	12.47	1.122	0.777	0.194	4.15	14.3	3.58
T ₁	Intermediate foidolite	18	0.67	1.37	2.22	3.85	16.51	0.949	1	0.243	4.26	31.2	7.56
T ₂	Mafic foidolite	28	0.46	1.42	2.18	5.16	17.60	0.862	0.996	0.192	3.89	25.6	4.93
T ₃	Ultramafic foidolite	70	0.10	1.06	2.44	3.97	9.64	0.656	1.253	0.151	4.23	68.0	8.18
(b) Volcanic rocks using TAS classification													
A	Silexite	116	0.078	0.44	1.28	2.81	6.28	-0.058	1.465	0.137	2.76	57.3	5.35
B	Rhyolite	10,015	0.70	1.71	2.51	3.69	6.35	0.877	0.698	0.007	3.07	5.92	0.059
C	Dacite	4820	0.26	0.66	1.25	1.98	3.35	0.098	0.827	0.012	1.55	2.37	0.034
D	Andesite	5058	0.16	0.44	0.78	1.22	2.43	-0.334	0.835	0.012	1.01	1.04	0.015
E	Basaltic andesite	8646	0.063	0.20	0.39	0.66	1.36	-1.057	0.932	0.010	0.54	0.40	0.0043
F	Subalkalic basalt	14,192	0.024	0.068	0.15	0.29	0.69	-1.952	1.058	0.009	0.25	0.13	0.0011
G	Picrobasalt	267	0.073	0.22	0.51	0.97	4.12	-0.71	1.415	0.087	1.34	11.5	0.70
I	Trachydacite	2083	0.75	1.49	2.16	3.24	5.88	0.784	0.677	0.015	2.76	4.41	0.097
J	Trachyte	1220	1.20	2.13	3.19	4.98	11.33	1.217	0.719	0.021	4.37	12.9	0.37
K	Trachyandesite	2905	0.57	0.96	1.55	2.52	5.40	0.463	0.773	0.014	2.14	3.75	0.070
L	Basaltic trachyandesite	3529	0.24	0.63	0.92	1.39	3.08	-0.098	0.786	0.013	1.24	1.31	0.022
M	Trachybasalt	3488	0.35	0.64	0.86	1.22	1.91	-0.15	0.567	0.010	1.01	0.39	0.007
N	Alkalic basalt	6608	0.16	0.35	0.54	0.78	1.58	-0.641	0.708	0.009	0.68	0.30	0.004
O	Phonolite	593	2.42	3.80	4.73	6.55	15.01	1.659	0.569	0.023	6.18	14.6	0.60
P	Tephriphonolite	255	1.29	2.47	3.42	5.08	9.78	1.275	0.63	0.040	4.37	9.28	0.58
Q	Phonotephrite	399	0.86	1.29	1.98	3.60	7.06	0.796	0.761	0.038	2.96	6.86	0.34
R	Tephrite	2637	0.53	0.85	1.13	1.51	2.72	0.153	0.614	0.012	1.41	0.91	0.018
S	Ultra-high alkali volcanic	16	2.54	3.09	3.44	4.20	5.01	1.257	0.211	0.054	3.60	0.59	0.15
T ₁	Intermediate foidite	48	0.70	2.07	3.33	5.92	12.33	1.175	0.814	0.119	4.51	19.1	2.79
T ₂	Mafic foidite	46	1.16	2.20	3.65	5.26	5.96	1.155	0.593	0.088	3.79	6.04	0.90
T ₃	Ultramafic foidite	133	0.79	1.09	1.51	2.66	4.65	0.584	0.863	0.075	2.60	7.50	0.65
U	Boninite	8	0.054	0.079	0.10	0.11	0.12	-2.39	0.284	0.107	0.095	0.0010	0.0004
V	Meimechite	20	0.072	0.10	0.21	0.42	1.09	-1.553	0.891	0.204	0.32	0.12	0.028
W	Komatiite	78	0.011	0.051	0.086	0.27	1.27	-2.244	1.26	0.144	0.23	0.21	0.024
X	Picrite	165	0.045	0.10	0.18	0.32	1.02	-1.732	1.101	0.086	0.32	0.25	0.019
Y	Alkali picrite	72	0.15	0.34	0.56	0.97	2.84	-0.517	0.884	0.105	0.88	0.92	0.11

sources and or formational processes (Frost et al., 2001). While the classification is typically applied to granitic rocks, we have applied it to all plutonic rocks as the composition of igneous rocks represents a continuum.

4. Results

4.1. Gross observations

The range and frequency of estimated physical properties are summarized in Fig. 4. Because heat production ranges over several orders of magnitude, we display the heat production data in log₁₀-space. Heat production estimates range from a maximum of 14,000 $\mu\text{W m}^{-3}$ to a minimum of 0.001 $\mu\text{W m}^{-3}$ that may be limited by detection limits. However, the vast majority of the data fall

between 0.01 and 30 $\mu\text{W m}^{-3}$ (Fig. 4a). The histogram of observed heat production peaks at a higher value for plutonic than volcanic rocks although the ranges are similar.

Seismic velocity and density estimates are bimodal, with peaks occurring at similar positions for both plutonic and volcanic samples (Fig. 4b and c). The heights of the dominant peaks are reversed between the plutonic and volcanic data. These data illustrate sampling within the database, but do not give us great insight into heat production without further compositional knowledge.

In Fig. 5, the three estimated physical properties are binned into 5 wt.% intervals of SiO₂ concentration. This result nicely illustrates the first-order compositional variations expressed through these physical properties. Density and seismic velocity generally increase as composition ranges from felsic to mafic (Fig. 5 center and right columns). In contrast, heat production decreases from felsic to

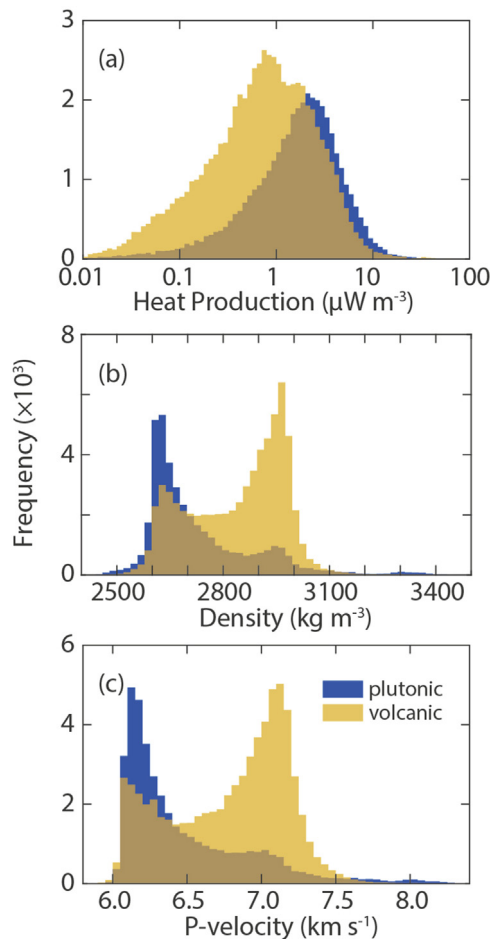


Figure 4. Distributions of estimated (a) heat production, (b) density, and (c) seismic velocity for plutonic (blue) and volcanic (orange) data.

mafic compositions, especially notable within the plutonic suite (Fig. 5 left column). Above 50 wt.% SiO_2 , the peak values for all three physical parameters show systematic trends. Density and seismic velocity are best described by a normal or bimodal distribution, whereas heat production is best described by a log-normal distribution. This log-normal behavior has been noted previously with respect to HPE's (Rudnick et al., 1998) and is true of trace elements generally.

Heat production distributions begin to display a more complex shape at <55 wt.% SiO_2 . Density and seismic velocity likewise show a more complex behavior, noticeable <65 wt.% SiO_2 (Fig. 5). This more complex behavior can be explained using a greater number of compositional parameters than SiO_2 alone.

4.2. Heat production versus major oxides

Heat production increases with increasing SiO_2 and K_2O concentration (Fig. 6). The increase with K_2O is unsurprising since K is itself a heat producing element. Heat production decreases with FeO^T , MgO , and CaO oxides which are commonly concentrated in denser and more mafic rocks and minerals and are negatively correlated with SiO_2 concentration. The remaining oxides show no clear variation with heat production due to more complex relationships with SiO_2 .

No trend appears in P_2O_5 (Fig. 6i) that is predominantly concentrated in apatite, a common U-bearing mineral. This lack of correlation occurs because P_2O_5 is generally low in abundance for both mafic and felsic rocks, but high in intermediate compositions. This requires that the higher heat production contribution of U to felsic rocks are more likely to be found in other minerals such as zircon, which is common in felsic rocks and has an average of approximately 88 ppm but can contain very high concentrations, >1000 ppm (Belousova et al., 2002). By comparison, whole rock values for plutonic rocks are typically are lower than 15 ppm U.

Overall, the heat production variations with major oxides mirror trends seen in the seismic velocity estimates (Figs. 6 and 7). To emphasize this similarity, we have reversed the direction of the velocity axes in Fig. 7. Hence, increases in heat production with increasing SiO_2 and K_2O and decreasing CaO , MgO , and FeO are reversed for seismic velocity. The similarities between SiO_2 , CaO , and MgO in particular—elements used to compute seismic velocity (Eq. (2))—bode well for a relationship between heat production and seismic velocity.

While we only present the oxide results for plutonic rocks, the observations are nearly identical for volcanic rocks. One exception is TiO_2 , which shows a slight decrease in heat production with increasing TiO_2 , which again, is less abundant in felsic compositions.

4.2.1. Heat production versus geochemical indices

Another common way to view the compositional space of igneous rocks are through the use of compositional indices, which combine elements in by mass or molar abundance in a specified way. Often these indices are used to classify rocks based on chemical trends, or emphasize certain processes. In this case, we use the geochemical indices to enhance the chemical trends seen in the oxide data. Fig. 8 shows the results of heat production with respect to five such chemical indices.

Heat production tends to increase as a function of the iron number, Fe^* , above a value of ~ 0.5 ; however, this increase is as much due to a significantly narrower range of Fe^* near a value of 1 (Fig. 8a and f). These high values of Fe^* are rarely seen outside of felsic rocks whereas mafic rocks may also have low values of Fe^* (Frost et al., 2001).

Heat production decreases as the maficity index increases for the majority of the sampled compositions (Fig. 8b and g). This result is relatively systematic for the bulk of data from index 0 to ~ 0.4 and confirms the observations made from the oxide data (Fig. 6). The relationship between heat production and maficity is nearly log-linear for volcanic rocks with maficity ranging from 0 to 0.4.

The clearest relationship between a geochemical index and heat production is found with the MALI index (Fig. 8d and i), for which heat production log-linearly increases with MALI over most of its range. On the basis of this observation, we can expect high-alkali rocks to have higher heat production than calcic rocks.

The ASI shows no clear trend from metaluminous, <1, to peraluminous values, >1 (Fig. 8c and h). However, a difference in median values is observable in the plutonic relative to the volcanic data. Volcanic rocks have median values near $\text{ASI} = 1$ that are lower in heat production than plutonic rocks. This observation likely reflects the sampling biases in the compositional space, with greater sampling of mafic volcanics and felsic plutonics.

The chemical index of alteration (CIA) expressed in molar form is optimally 50 for peraluminous igneous rocks, but increases in response to chemical weathering (Goldberg and Humayun, 2010). Since most values in this dataset are near or below 50, it is clear

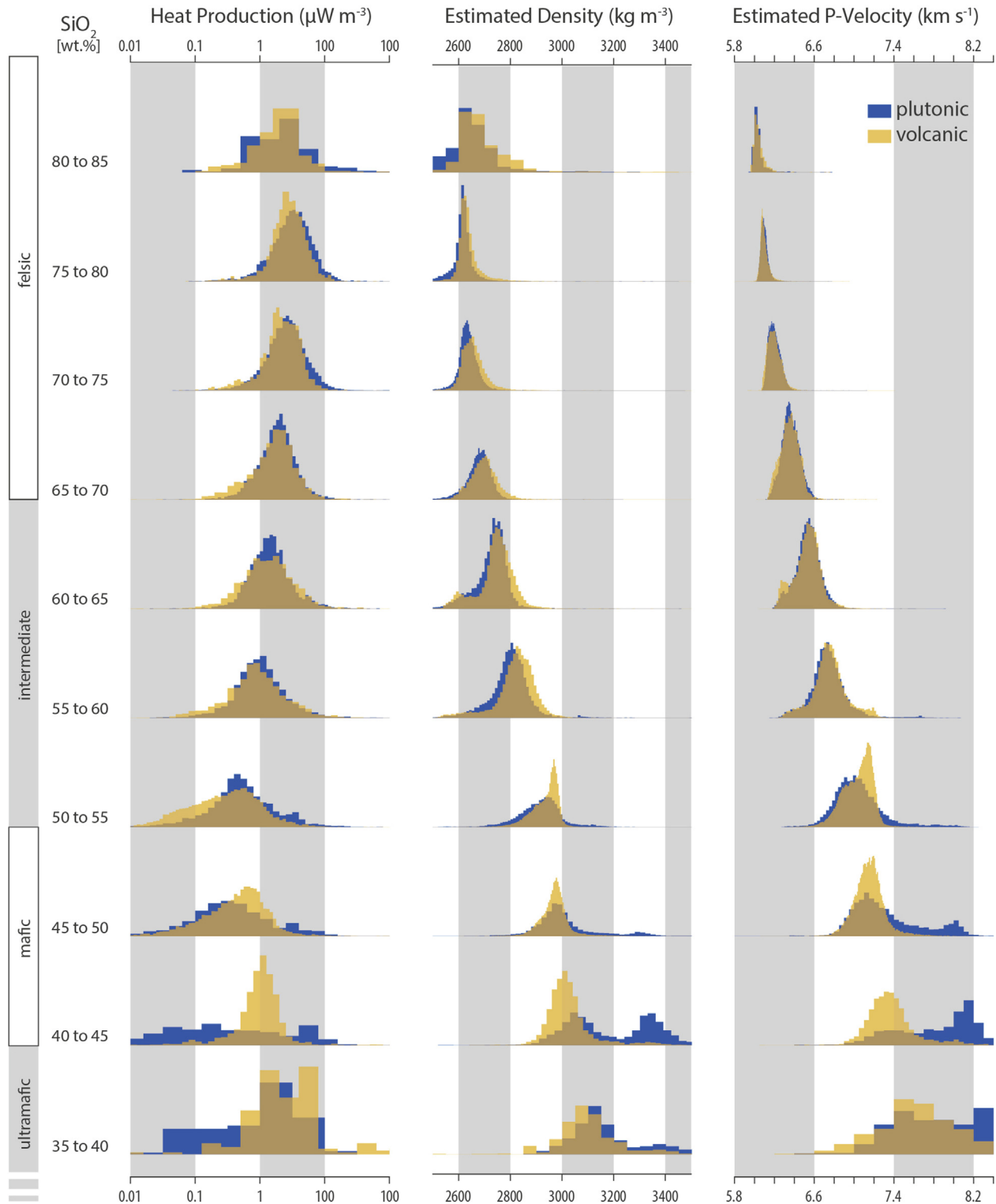


Figure 5. Distributions of heat production (left column), estimated density (center column) and estimated *P*-wave velocity (right column) for plutonic (blue) and volcanic (orange) rocks. The data are divided into 5 wt.% intervals of SiO₂ concentration.

that most of the rocks in the databases are relatively fresh (Fig. 8e and j). While CIA is relatively similar in formulation to ASI, there is a more consistent pattern in the CIA. There is a slight increase in heat production as CIA increases up to a value of 50, but remains relative constant above 50. In the range covering the bulk of the

data (0.35 to 0.6), the trend in median values is again nearly log-linear.

As mentioned previously, the heat production is displayed in log₁₀-space, which means the log-linear relationships mentioned above are exponential in linear-heat-production-space.

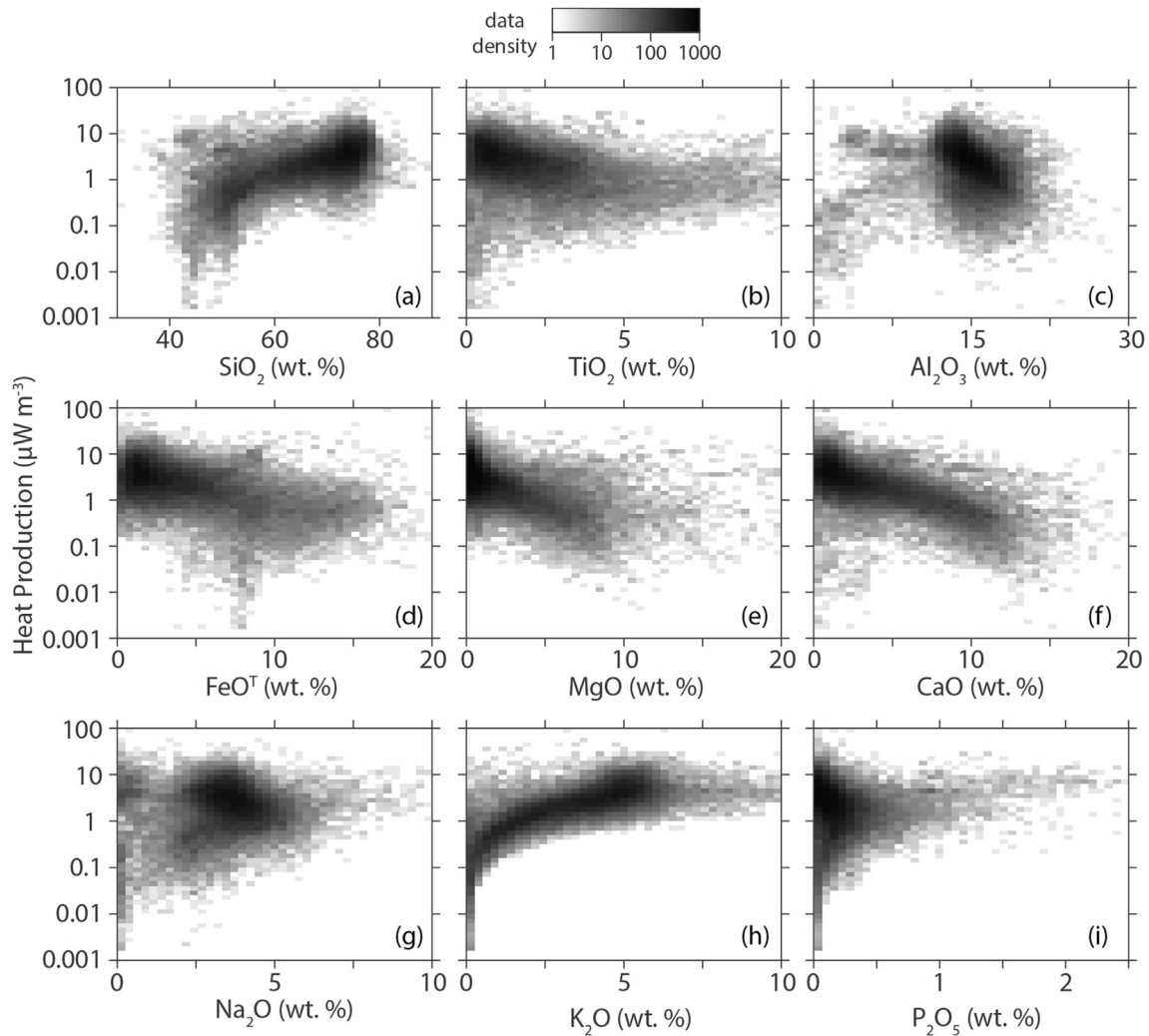


Figure 6. Heat production as a function of major oxides in plutonic rocks. The shading indicates logarithmic data frequency within each 2D bin.

4.3. Heat production and SIA classification

Using Fe^* and ASI, we separate the suite of igneous rocks into A-type (ferroan), S-type (magnesian, peraluminous), and I-type (magnesian, metaluminous) as defined by Frost et al. (2001). Because seismic velocity systematically varies with SiO_2 content, we can use V_p loosely as a proxy for SiO_2 . Using seismic velocity as a second variable allows us to spread the heat production variations across several histograms reducing the influence of sampling bias (e.g. the high number of mafic volcanics).

The results for SIA classification are fairly similar for both plutonic and volcanic rocks (Fig. 9). S- and A-type rocks account for the bulk of the data for seismic velocities $<7.4 \text{ km s}^{-1}$ whereas I-type rocks account for most of the data $>7.4 \text{ km s}^{-1}$. Heat production is generally high when seismic velocity is low, which corresponds to more felsic compositions. Heat production is low when seismic velocity is high, corresponding to more mafic compositions.

The natural variability of heat production is generally low among the S-type and A-type relative to the I-type, especially samples at higher velocities. Median heat production for S- and A-type igneous rocks are clearly defined by log-linear trends from 6.0 to 7.4 km s^{-1} (Fig. 9). While heat production generally decreases

with seismic velocity for I-type rocks, there is not a clear relationship between these two estimated parameters (Fig. 9).

In addition to Fe^* and ASI, the igneous classification scheme by Frost et al. (2001) adds MALI as a chemical discriminator. Consistent with the high correlation between heat production and MALI, we observe variations among igneous rocks between the alkali to calcic subclasses that are not readily apparent in the SIA classification. For instance, the magnesian peraluminous samples (S-type) show a gradual increase in median heat production from calcic to calc-alkalic to alkali-calcic to alkalic with little variation in slope. A similar observation is made within the ferroan metaluminous and ferroan peraluminous (both A-type) igneous samples.

The magnesian metaluminous (I-type) series are less commonly observed. Median estimates for the calc-alkalic and calcic I-type subclasses are similar in slope (decreasing heat production with increasing velocity) as the ferroan and magnesian peraluminous data. The magnesian metaluminous alkalic and alkali-calcic data appear fundamentally different with relatively constant median heat production from low to high estimated seismic velocity. When mixed with the calc-alkalic and calcic subclasses, these high heat producing mafic subclasses create the high variability observed within I-type rocks.

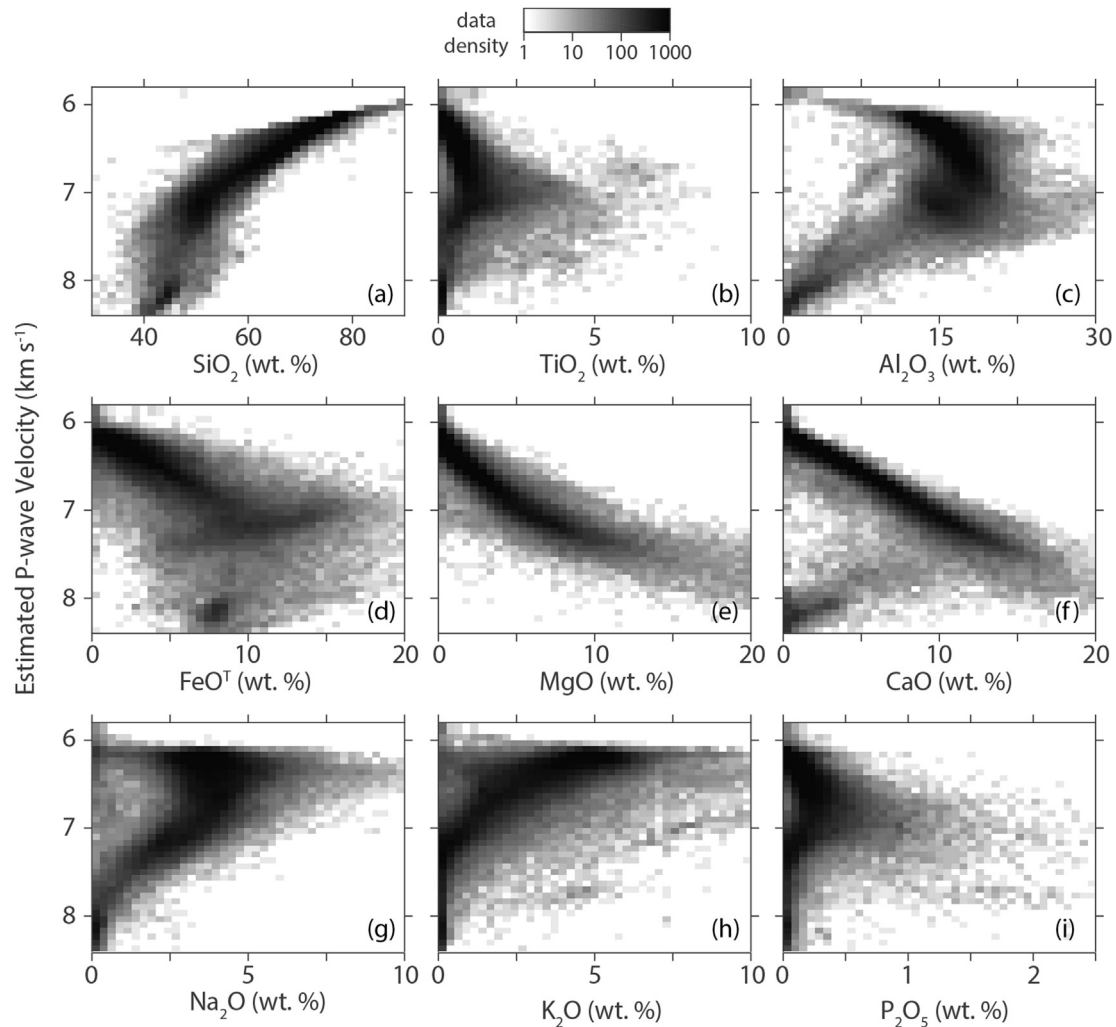


Figure 7. Estimated P-wave velocity as a function of major oxides in plutonic rocks. The shading indicates logarithmic data frequency within each 2D bin. Note that the vertical axis has been reversed (low velocities at top) to emphasize the similarity to heat production estimates (Fig. 6).

4.4. Heat production and TAS classification

Based on the results above, we expect mafic and subalkaline rocks to have lower heat production on average than felsic and more alkaline ones. Indeed, by compositionally classifying rocks into the commonly used TAS fields, we find both of these trends are clearly observable (Table 4). By combining the TAS fields with density and seismic velocity we can see directly how these chemical variations are related to geophysical quantities that can be estimated more readily from data collected at Earth's surface (Fig. 10).

The relationship between felsic–mafic compositions, heat production, density and seismic velocity is apparent in Fig. 10. Both plutonic and volcanic rocks trend from low heat production, high velocity within ultramafic compositions to high heat production, low velocity within felsic rocks.

For most rock types, 90% of $\log_{10}A$ estimates vary approximately one order of magnitude and V_p by 0.5 km s^{-1} . Data ranges for the middle 50% of the data are about half as large as they are for 90% interquartile range. Rocks high in SiO_2 , such as granites and rhyolites, are the slowest seismically and have the highest heat production.

Superimposed on this trend is the additional effect of the alkaline ($\text{K}_2\text{O} + \text{Na}_2\text{O}$) content (Fig. 10a–d). Subalkaline rocks (A to

G, H and U to X) have systematically lower heat production than alkaline rocks (I to T and Y). From Fig. 6 it is clear that it is K_2O —a heat producing element—that correlates with heat production whereas Na_2O does not. Hence, it is the K_2O that dominates the subalkaline to alkaline trends and Na_2O that adds to the variability of individual rocks types due to the definition of the TAS classification scheme.

Subalkaline trends in heat production with estimated seismic velocity are nearly log-linear except for a drop in heat production for the most silica rich rocks $>90 \text{ SiO}_2$ (Fig. 10a and c, A–H). These quartzolites and silexites (Fig. 10a and c, field A) are exceptionally quartz-rich, representing hydrothermal veins or the extreme end of fractional crystallization processes—often identified as samples from pegmatites—which solidify after some of the HPEs have been removed from the melt. Additional log-linear trends are observed in alkaline series subparallel to the subalkaline trend (Fig. 10a and c, I–N and O–R), particularly within the volcanic data.

The high-Mg volcanics (fields U to W, Fig. 10a and c) tend to have higher estimated seismic velocities than low-Mg volcanics with similar values of SiO_2 . These rocks also tend to have among the lowest heat production consistent with the general pattern with respect to velocity but not SiO_2 content.

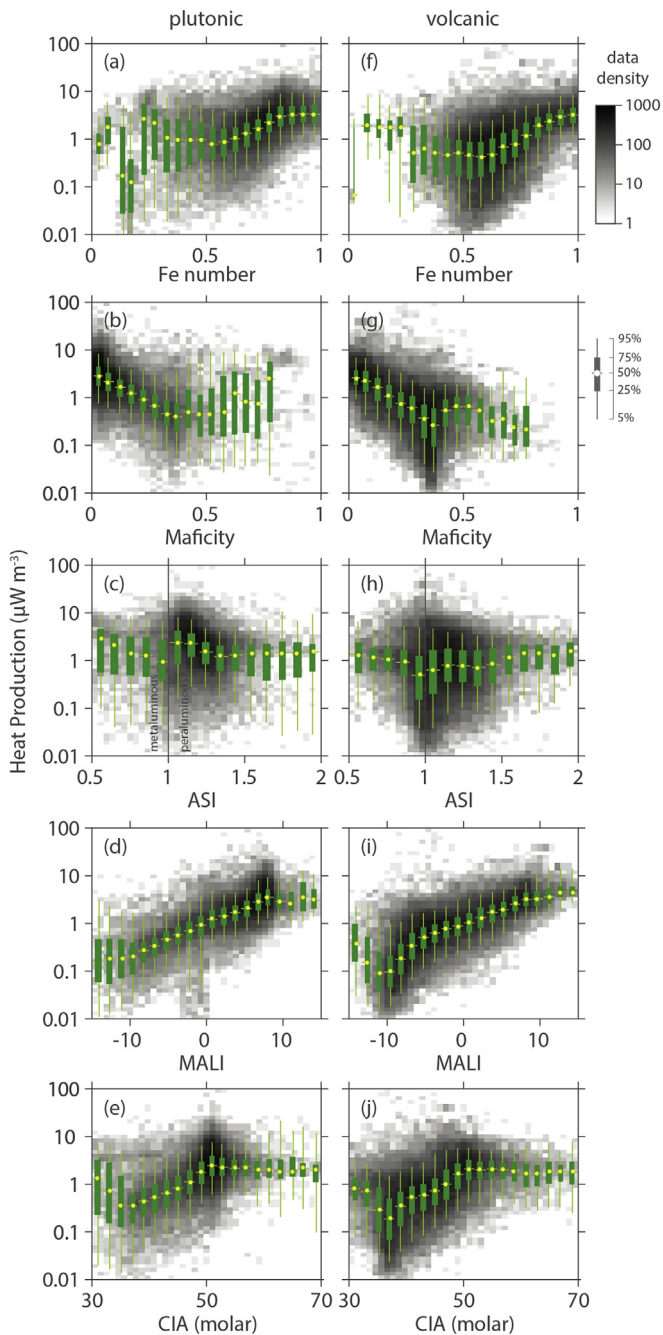


Figure 8. Heat production as a function of geochemical indices for plutonic rocks (a–e) and volcanic rocks (f–j). The data are presented as a 2D histogram and shaded according to the data density along a logarithmic color scale. The data are also divided into bins of equal size for each of the respective geochemical indices, where the central dot represents the median value, the size of the box represents the 25 to 75% quantiles and the whiskers extend to the 5 and 95% quantiles. The solid vertical line (c, h) represents the classification division between peraluminous (ASI > 1) and metaluminous (ASI < 1) rocks (Frost et al., 2001). The chemical index of alteration, (e, j) is computed by $CIA = 100n_{Al_2O_3} / (n_{CaO} + n_{Na_2O} + n_{K_2O})^{-1}$, where $n_{CaO} = n_{CaO} - 10/3n_{P_2O_5}$. Generally, CaO^+ includes an additional correction for CO_2 in silicates, but CO_2 is not reported for a large fraction of the dataset so we do not include this term for consistency.

5. Discussion

5.1. Natural variability and uncertainty

Our analysis of this geochemical data compilation provide rigorous bounds on the average heat production and the natural

variability of igneous rocks by type and chemistry. The use of a significantly larger database than previous studies allows for some generalizations to be made from these data that were not possible or were less apparent in previous studies.

The natural variability of heat production for most rock types varies between one and two orders of magnitude (Table 4); however, the uncertainty in the average is far smaller. Due to the large number of samples, two standard errors of the mean is no greater than the size of the symbols used to plot the median (Table 4 and Fig. 10). The large natural variability in the heat production of hand samples suggest that it may be difficult to estimate the heat production of any individual sample, but the distributions for each rock type may be used to define a priori distributions for use in Bayesian-based modeling studies.

While the natural variability is generally high for hand samples, variability is dependent upon the scale of investigation. The natural variability among plutons is smaller than that observed within individual hand samples.

To put this in perspective, consider heat production variations at the grain scale. Grains of zircon and monazite can have very large heat production $>1000 \mu W m^{-3}$ that varies greatly from grain to grain (Belousova et al., 2002). Therefore at the scale a chemical analysis is made, the heat production is highly dependent upon the number and magnitude of the zircons grains it contains, which will vary considerably from analysis to analysis. Given a sufficiently large number of analyses on the same hand sample one will be able to accurately and precisely estimate the average heat production of the hand sample from which they originate despite a large natural variability at the scale of a single analysis. Portions of hand samples are crushed and homogenized prior to analysis to dampen this nugget effect.

Likewise, the uncertainty in the average heat production of an outcrop will be smaller than the natural variability of the individual hand samples from which the estimate is based. Thus, the uncertainty in the average heat production of a pluton will be smaller than the combined variability from the individual hand samples that are used to determine its average.

Given that the range in average heat production between various continents and geologic provinces regardless of composition are relatively small (Section 5.3.2), we suggest that the predictive power of seismic velocity–heat production models are significantly more certain than one would assume from on the natural variability of hand samples. Therefore these models can be used effectively to estimate the heat production distribution within the lithosphere at scales sufficient for regional and global modeling studies. Unfortunately, no study at present exists which examines the variability of heat production at multiple scales. Such a study would help us gauge how much smaller an uncertainty we could expect for a regional-scale heat production estimate derived from hand samples with large natural variability.

5.2. Linear V_p – $\log_{10}A$ relationships

We develop several log-linear relationships between seismic velocity and heat production. In addition to the chemically based models developed for the full global dataset (Fig. 9), we split the data geographically to explore the viability of such models on geographic basis. While the natural variability is clearly high for heat production, we show that the median values are both well-behaved and relatively well-defined regardless of how the data are split.

It is clear from our results that median heat production and median seismic velocity are correlated, validating the earlier attempts by Rybach and Buntebarth (1982, 1984). We do not suggest that this correlation results from a direct causal relationship

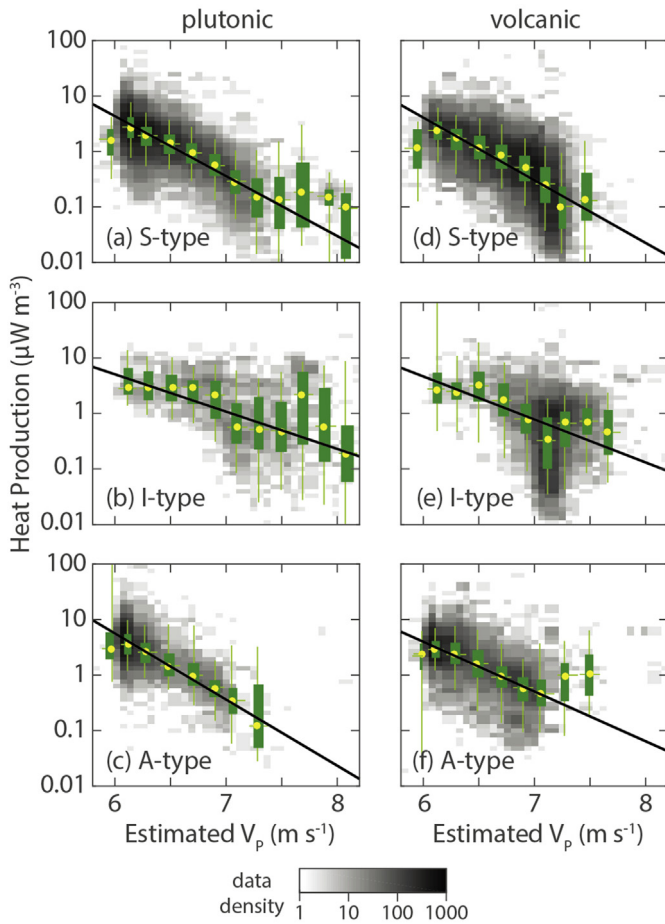


Figure 9. Heat production sorted by geochemical classification of granitic rocks extended to all plutonic rocks (a–c) and volcanic rocks (d–f). Shading and whisker plots are produced in the same manner as in Fig. 8. Linear models are calibrated to median values between 6 and 7.4 km s⁻¹ except volcanic A-type which is calibrated between 6 and 7.2 km s⁻¹ (Table 5).

between the two parameters, but merely provides a basis from which heat production may be empirically estimated from seismic velocity. The difficulty with developing a physically-based model are well-documented. For instance, Fountain (1987) suggested the large natural variability in heat production exists due to the dependence upon the source chemistry, creation and subsequent evolution/alteration.

Globally, the average behavior of seismic velocity and density are highly correlated to heat production (Figs. 9 and 10a,c). For seismic velocities between 6.0 and 7.4 km s⁻¹, the log-linear correlation coefficient between median log₁₀A and V_p is -0.992 for plutonic rocks and -0.980 for volcanic rocks. This restricted range accounts for ~95% of plutonic data and ~97% of volcanic data. Likewise, between 2600 and 3000 kg m⁻³ correlation coefficients for median log₁₀A to density is -0.989 for both plutonic and volcanic rocks. This range accounts for ~86% of plutonic data and ~93% of volcanic data.

Since correlation coefficients are high, we use log-linear models to estimate heat production from estimated seismic velocity. We compute several linear models between median V_p and median log₁₀A for subsets of the data (Table 5). The log-linear model is shifted so that the intercept occurs at 6 km s⁻¹, i.e.,

$$\log_{10}A = m(V_p - 6) + b \quad (4)$$

Note, this is equivalent to an exponential relationship, $A = 10^{b/10m(V_p-6)}$. By shifting the data, we consider the intercept of the lines to approximate the peak in heat production expected for felsic composition that occurs at ~6.0 km s⁻¹ (e.g., Figs. 9 and 10a,c).

The r² values for log-linear models of the data subsets are generally high, >0.9, for all but high-alkaline plutonics and I-type rocks (Table 5). The r² is lower for the high-alkaline data because there are too few data and the natural variability is too great to more precisely constrain averages. For I-type rocks, the decrease is due to the high variability in heat production at high seismic velocities.

The intercept is sensitive to the alkalinity, which increases for both volcanic and plutonic rocks from ~3.89 to >9 μW m⁻³ (Table 5). Uncertainties on the intercept values are generally less than 0.1 log-units. For the 3.89 μW m⁻³ subalkaline intercept, this translates to 95% confidence between 3.24 and 4.67 μW m⁻³. For S-, I-, and A-types, the intercepts lie between 4.0 and 5.6 μW m⁻³ but are not consistent between volcanic and plutonic samples of the same type. The differences between volcanic and plutonic averages reflect the averaging of igneous rock samples with varying degrees of alkalinity.

Slopes range from -0.7 to -1.2 log₁₀[(μW m⁻³)(km s⁻¹)⁻¹] with a general uncertainty of about ±0.1. No general rule can be established for differences between volcanic and plutonic rocks. However, the subalkaline and alkaline trends are the least affected by sampling bias and yield very similar results for plutonic and volcanic rocks. We interpret this result as an indication that the average compositional behavior for heat production is similar for both plutonic and volcanic rocks.

The subalkalic heat production model is consistent with heat production from mantle samples in this databases, but there are reasons to suspect it may be lower. The subalkaline heat production model predicts a heat production of 0.002 μW m⁻³ at 8.2 km s⁻¹, consistent with typically quoted estimated for the continental lithosphere, ~0.02 μW m⁻³, based on larger xenolith databases (Rudnick et al., 1998; Hasterok and Chapman, 2011). This result is significantly smaller than our estimate for mantle peridotite (median 0.013 μW m⁻³, Field H₂ in Fig. 10a). Metasomatic enrichment of heat producing elements in mantle samples from kimberlite hosted xenoliths (Dawson, 1984), could account for the high heat production estimate, but it is more likely the small dataset from which our estimates are derived. Therefore, we suggest these lower values from previous studies are preferable to the estimates produced in this study.

Density is also be log-linearly related to heat production over a similarly restricted range (2600 to 3000 kg m⁻³). The global trends for heat production and density are very similar for both plutonic and volcanic samples. The average log-linear relationship between heat production and density is

$$\log_{10}A = -0.0027(\rho - 2700) + 0.53 \quad (5)$$

where A is in μW m⁻³ and ρ is in kg m⁻³. Uncertainty in the slope is approximately ±0.0004 (log₁₀μW m⁻³)(kg m⁻³)⁻¹ and intercept, ±0.10 μW m⁻³. Below 2600 kg m⁻³, heat production decreases due to the increasing purity of SiO₂-rich samples.

Because both seismic velocity and density depend upon major element concentrations and volumetric heat production depends upon density as well as trace element concentrations (Eq. (1)), there is a concern that the log-linear relationship is an artifact from the use of thermodynamic property estimates. Since major and trace elements are generally viewed as uncorrelated (Fountain, 1987), we need to demonstrate that this relationship is not an artifact of the modeling process.

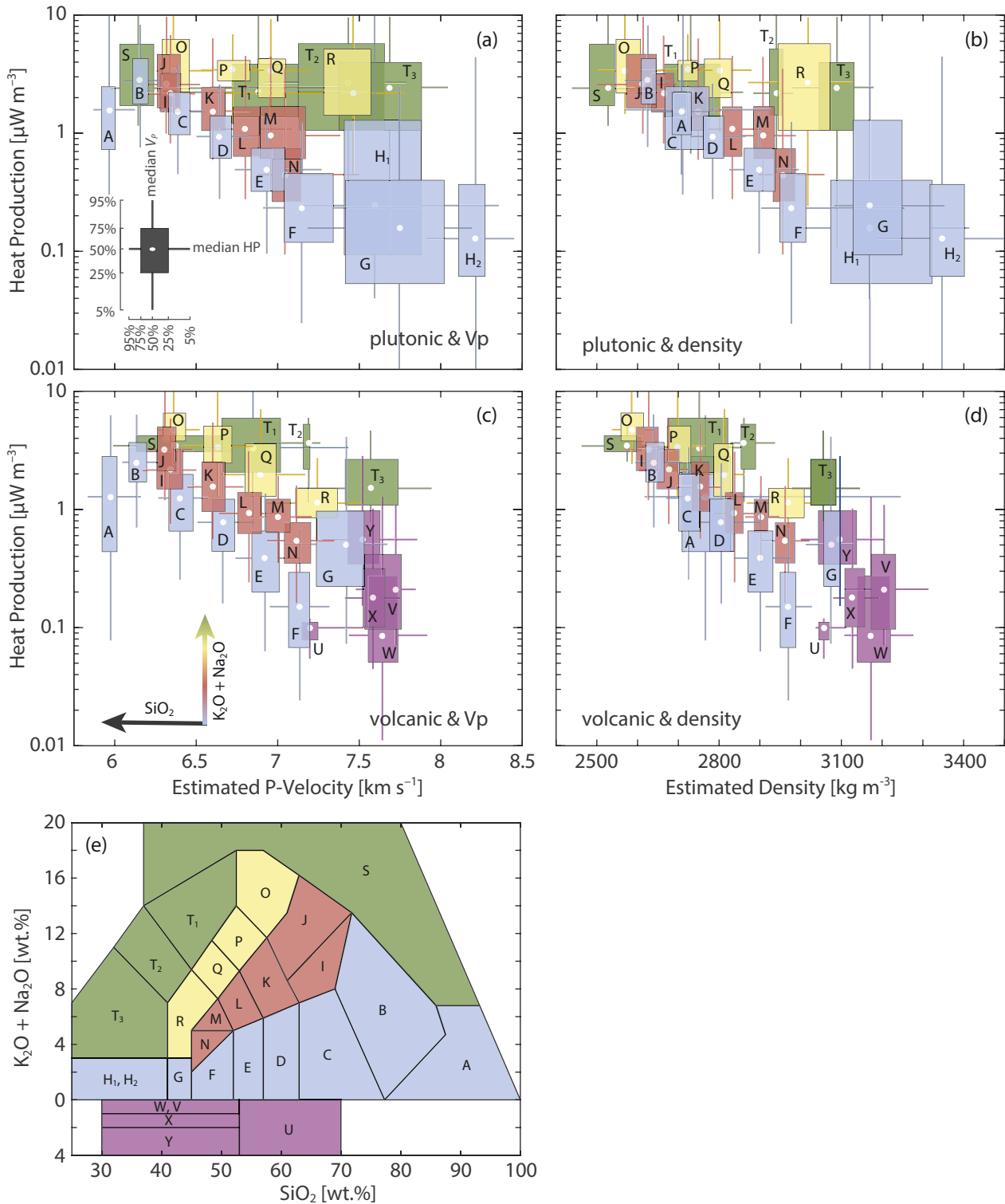


Figure 10. Heat production as a function of seismic velocity (a, b) and density (c, d) for plutonic (a, c) and volcanic (b, d) rocks determined by the (e) TAS classification scheme (modified from Mittlemost, 1994). For values and a description of rock fields, see Tables 3 and 4. Field H₁ (cumulate peridotite) is separate from H₂ (mantle peridotite) on the basis of Mg# < 80. Fields U (boninite), V (meimechite) and W (komatiite) have high MgO and V is further separated from W by TiO₂ > 1 wt.% (Le Bas and Streckeisen, 1991). Whisker plots are by the quantiles shown as inset in (a).

There are two ways we can show that the log-linear relationships are not an artifact of the modeling. First, the definition of volumetric heat production (Eq. (1)) predicts a positive slope between heat production and density (i.e., heat production should decrease with density as silicic content increases). Instead, we find

a negative slope. Therefore, it is the concentration of HPE's that clearly dominate the magnitude of heat production and not the major elements that control density and seismic velocity.

Second, if density is excluded from the computation of heat production (Eq. (1)) then we estimate the heat production by mass.

Table 5
Linear models^a of heat production versus seismic velocity.

Log-linear model	N	$2\sigma_m$		$2\sigma_b$		r^2	Figure
		$[\log_{10}(\mu\text{W m}^{-3})]$	$(\text{km s}^{-1})^{-1}$	$[\log_{10}(\mu\text{W m}^{-3})]$	$(\mu\text{W m}^{-3})$		
<i>Plutonic models</i>							
Subalkaline (B to F)	31,294	-1.04	0.06	0.61	0.04	0.991	10a
Alkaline (G, I to N)	7277	-0.84	0.07	0.67	0.07	0.967	10a
High alkaline (O to R)	1061	-0.09	0.05	0.59	0.05	0.662	10a
S-type	26,737	-1.08	0.07	0.64	0.05	0.978	9a
I-type	3367	-0.67	0.20	0.70	0.16	0.689	9b
A-type	9958	-1.19	0.09	0.75	0.07	0.971	9c
Oceanic	659	-1.33	0.17	0.79	0.13	0.928	11a
Continental	39,887	-0.92	0.04	0.60	0.04	0.988	11a
Australia	12,510	-0.92	0.07	0.73	0.05	0.975	12a
Finland	2744	-0.89	0.10	0.52	0.08	0.944	12a
North America	22,789	-1.04	0.05	0.62	0.04	0.975	12a
<i>Volcanic models</i>							
Subalkaline (B to F)	42,731	-1.16	0.10	0.59	0.08	0.977	10c
Alkaline (G, I to N)	20,100	-0.71	0.08	0.62	0.07	0.935	10c
High alkaline (O to R)	3884	-0.72	0.05	0.96	0.04	0.992	10c
S-type	38,452	-1.13	0.13	0.61	0.10	0.942	9d
I-type	14,494	-0.77	0.18	0.67	0.15	0.780	9e
A-type ^b	18,367	-0.90	0.04	0.60	0.03	0.990	9f
Oceanic	13,356	-1.12	0.14	0.57	0.11	0.929	11c
Continental	54,411	-0.70	0.10	0.48	0.08	0.905	11c
Australia	6814	-0.57	0.11	0.53	0.09	0.845	12c
Finland	744	-1.00	0.12	0.49	0.10	0.929	12c
North America	15,984	-0.77	0.08	0.47	0.06	0.954	12c

^a Models are fit to median binned data and restricted to V_p between 6.0 and 7.4 km s^{-1} . The log-linear model is of the form $\log_{10}A = m(V_p - 6) + b$.

^b Model is fit to median binned data and restricted to V_p between 6.0 and 7.2 km s^{-1} because the model is otherwise highly skewed by the relatively few data that define the median above 7.2 km s^{-1} (Fig. 9).

Since this definition decouples any dependence of heat production on major elements, it is difficult to see how an artifact could be created accidentally by our modeling process if the major elements and trace elements were not correlated on average. When we use the heat production by mass, we find that the correlation coefficients are the same or improve very slightly (r^2 increases by <0.005) for all cases. The slight improvement in correlation coefficient occurs because the heat production observations no longer include uncertainties contributed by the density estimate.

5.3. Geographic variations in heat production and log-linear models

Heat production varies geographically (Fig. 1). Much of this variation results from the dominant rock types found within a given region, but there are more subtle variations between regions. The models presented above are useful if the chemistry of the lithosphere can be linked to a specific compositional series or igneous type. However, lithospheric chemistry, architecture, and history are generally complex.

Because the natural variability is large, we need to know if the log-linear trend between heat production and seismic velocity is reflective of the global average alone, or whether it can be used to realistically estimate the average heat production in geographically smaller settings. The former case only permits loose bounds on heat production whereas the latter case allows development of higher resolution models tailored to individual regions so that they

better represent the spatial/volumetric average of lithospheric composition.

To test whether the log-linear relationship is valid on subsets of dataset, we separate the data by oceanic and continental domains (Fig. 11) and examine continent-wide data (Fig. 12). The high correlation coefficients between median values still allow for an accurate estimate of the average heat production from seismic velocity in each of these regions (Table 5).

5.3.1. Oceanic and continental heat production

The ranges of oceanic and continental heat production largely overlap. However, Fig. 11 shows a very slight, but persistent reduction in median heat production of oceanic relative to continental rocks for most seismic velocity bins ranging from 6 to 7.0 km s^{-1} . Over this range of velocities, we expect the slope to be relatively similar for both settings. However, the estimated slope is much higher for oceanic than continental rocks (Fig. 11).

Heat production of mafic (high velocity) rocks within the oceanic domain are significantly lower than similar continental rocks, which accounts for the difference in slope (Table 5). While

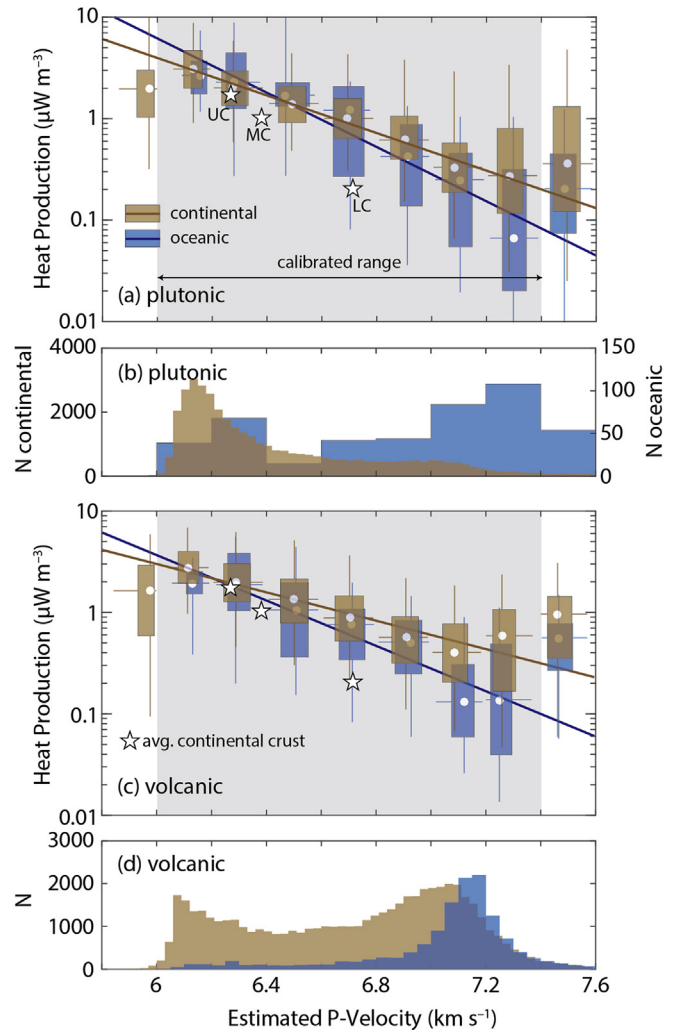


Figure 11. Heat production and estimated seismic velocity within continental and oceanic settings for (a) plutonic and (c) volcanic rocks. The log-linear models are calibrated to median values between 6 and 7.4 km s^{-1} (Table 5). The stars represent the estimates for the global average upper crust (UC), middle crust (MC) and lower crust (LC) compositions from Rudnick and Gao (2003). The number of data within each subset are shown in (b) and (d).

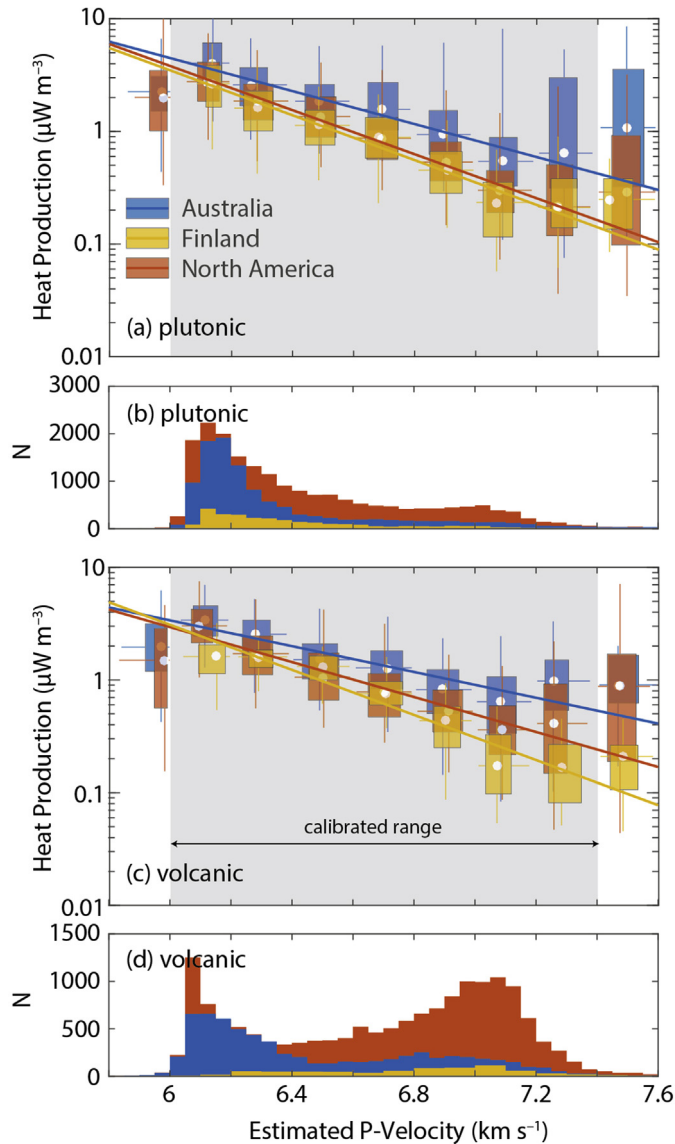


Figure 12. Geographical subsets of heat production and estimated seismic velocity for (a) plutonic and (c) volcanic rocks. The log-linear models are calibrated to median values between 6 and 7.4 km s^{-1} (Table 5). The number of data within each subset are shown in (b) and (d).

there are relatively few oceanic plutonic rocks, the results are similar to the better sampled volcanics. Therefore, the differences in slopes for the oceanic and continental domains are not simply the result of sampling.

Examining basaltic distributions in greater detail (Fig. 13), it appears that the source of the continental/oceanic difference lies with the heat production of subalkalic basalts which have lower heat production within the oceans. Alkali basalts on the other hand are relatively similar between the oceanic and continental domains. The geographic distribution of the two basalt types are relatively similar, although the subalkalic data are more heavily weighted to mid-ocean ridges and the alkalic data include a greater proportion of oceanic plateaus which contain a more enriched source than mid-ocean ridge basalts (Humphreys and Niu, 2009). Assuming the sampling of the oceanic floor and continents are relatively representative of the spatial average of each domain, subalkalic basalts represent a larger ratio of all oceanic basalts (77%) compared to a

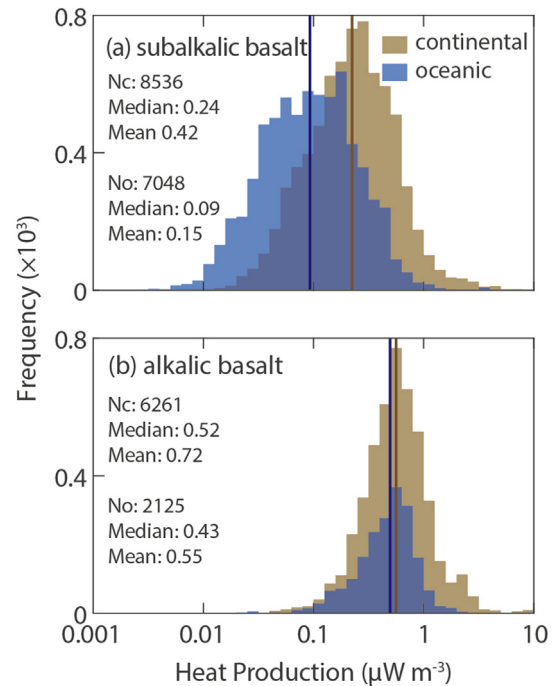


Figure 13. The distribution of oceanic and continental basalt heat production. Median values for each distribution are identified by the vertical lines.

similar ratio derived from continental samples (63%). The lower heat production of subalkalic relative to alkalic basalts further reduces the average heat production of oceanic relative to continental heat production at high seismic velocities.

5.3.2. Variations in continental heat production

Two of the better sampled continental regions include North America (United States, Canada and Mexico) and Australia. We use these data to explore for differences in continent-wide calibrated models, which we suspect on the basis of previous thermoistostatic studies (Hasterok and Chapman, 2011; Hasterok and Gard, 2016). Direct observations of heat production within Australia and high surface heat flow typically indicate high crustal radioactivity relative to the global average (Neumann et al., 2000; McLaren et al., 2003). These high heat has lead some to comment on the anomalous nature Australian heat production (Neumann et al., 2000; McLaren et al., 2003).

Heat production of Australian granites are in fact higher on average than North American granites, but there is significant overlap to the range (Fig. 14b and c). In addition, examination of the global heat production distribution of granites, the distribution is nicely log-normal; there is no peak that can be clearly identified as the Australian granites (Fig. 14a). This observation suggests that the higher heat production of Australian granites, while very high, may simply represent the higher end of the natural distribution.

Beyond simply granites, we find systematically higher median heat production in Australia relative to North America between 6.0 and 7.4 km s^{-1} (Fig. 12). Linear fits to the seismic velocity between 6.0 and 7.4 km s^{-1} yield a higher intercept for both plutonic and volcanic rocks but similar slopes between the plutonic rocks of each continent. The slopes of volcanic rocks, while similar between continents is lower than that of plutonic rocks (Fig. 12). Because these differences are systematic, we suggest that the high Australian heat production is due to crustal enrichment that likely extends vertically throughout the crust and possibly the entire lithosphere rather than simply enrichment of upper crustal felsic rocks that

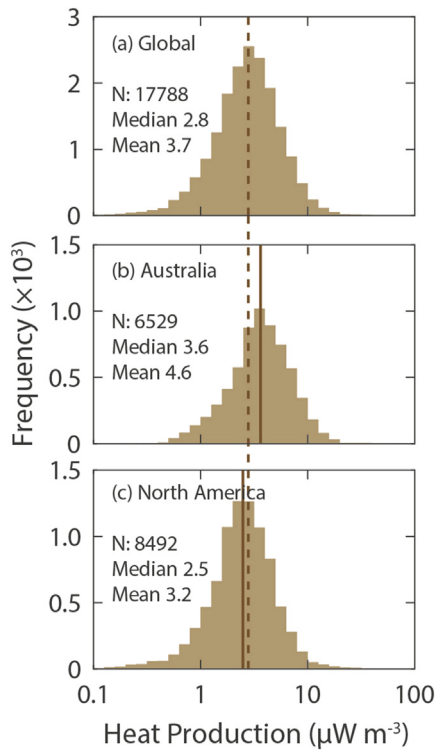


Figure 14. Heat production of granites (a) globally and within (b) Australia and (c) North America. Lines indicate values of median heat production, with the dashed line across all three histograms at the median of the global heat production distribution.

reflect the level of crustal differentiation. It should also be noted that the high Australian heat production need not be uniform across the continent, but is likely concentrated more regionally (Hasterok and Gard, 2016). Future work will investigate regional variations in the Australian lithosphere using this dataset.

Since these continent-wide subsets show distinct differences it is useful to determine if this log-linear relationship is valid at smaller scales, for example, a portion of a geological province. Finland, while containing considerably fewer data than North America or Australia, was subject to a campaign of relatively uniform geographic geochemical sampling that minimizes spatial bias (Rasilainen et al., 2007). As a result, we consider Finland a good test of regional variations that lie within a single geological province. The results from Finland are very encouraging as a test of regionally calibrated heat production–seismic velocity relationships as the natural ranges are smaller than the continent-wide observations (Fig. 12) and yield high log-linear correlation ($r^2 > 0.95$, Table 5).

The empirical relationship estimated for Finland results in a very similar slopes to both Australia and North America as well as the continents as a whole (Table 5 and Fig. 12). The estimated slopes for all our continental plutonic models lie between -0.89 and -1.04 $\log_{10}[(\mu\text{W m}^{-3})(\text{km s}^{-1})^{-1}]$, which are also similar to the estimates (between -1.19 and -0.84) for the Alps Rybach and Buntebarth (1984).

For most geological provinces, we find that estimates of the coefficient of determination (r^2) for log-linear models range from near zero to near unity when there are relatively few samples < 200 . As sample numbers increase, r^2 tends towards towards higher values. For ~ 1000 samples, $r^2 > 0.69$. While many regions with fewer than ~ 1000 samples have high correlation to log-linear models, the log-linear models may not be reliable as the coefficients determined for these models wildly vary. Over-sampling of a few outcropping units may lead to these high

correlation coefficients by chance, but not be representative of the province. This issue is less common for geologic provinces with a large number of samples.

Inspection of plutonic rocks for individual North American geological provinces with ~ 1000 samples, we find the data are well-correlated to a log-linear model, $r^2 > 0.69$ (Fig. 15). For those provinces with $r^2 > 0.9$ (four of the six), the estimated slopes (-0.98 and -1.14 $\log_{10}[(\mu\text{W m}^{-3})(\text{km s}^{-1})^{-1}]$) are consistent with the continent-wide models discussed above as well as Finland and the Alps. Therefore, the plutonic heat production differences between geological provinces may be dominantly expressed in the intercept value. In general, the range of heat production values are smaller than the continent-wide models, indicating higher certainty in the log-linear relationships observed for individual geological provinces.

The Northern Basin and Range and Southern Appalachian Mountains have lower correlation coefficients ($0.69 < r^2 < 0.9$), and lower slopes than those with higher correlation coefficients. The lower slope for these two regions may result from sparse sampling of some compositions, as several consecutive bins within both provinces appear to have higher slopes consistent with a higher sloped model (Fig. 15c and d). The Southern Appalachians for instance have lower heat production for slow velocity rocks (< 6.4 km s^{-1}) than we would expect for a slope of -0.9 to -1 . But the rocks with velocities from 6.4 to 7.4 km s^{-1} are reasonably fit by the higher slope.

5.4. Comparison to average continental crust

We can compare our results for the continental crust with average compositions estimated from previous studies (Rudnick and Gao, 2003, and references therein). To do so, we compute physical properties using the average crustal compositions in the same manner with which we estimate the individual samples in this study (stars in Fig. 11).

The upper and middle crust from (Rudnick and Gao, 2003) are consistent with our median estimates from our igneous samples. However, their lower crustal composition estimate results in considerably lower than our average continental heat production–seismic velocity model predicts (Fig. 11). Since we use the same method to estimate physical parameters for the average continental crust as for the rocks in this study, any errors or uncertainty in the parameter estimates apply to both models equally, and therefore, cannot cause of this difference.

Limiting our study to igneous rocks alone is a possible source for disagreement between our continental heat production–velocity model and the model lower crustal average. Incorporating metamorphic rocks which constitute a significant volumetric fraction of the continental crust may account for this discrepancy. However, preliminary estimates for metamorphic rocks suggest this is not the source and will be discussed as part of a future study.

Our continental model is based on predominantly surficial and a few drill core samples that are not uniformly distributed around the globe, which could result in spatial bias that creates a mismatch with average composition models. However, we consider this unlikely because the intercontinental variations which subset the model results in shifts of the intercept value, but are quite consistent in slope (Table 5 and Fig. 12). This consistent slope occurs regardless of the complex and disparate tectonic and magmatic histories amalgamating these individual regions. Therefore, we are fairly confident in the slope of our continental igneous model. A shift in the continental heat production model that fits the lower crust and accounts for a potential bias cannot fit the upper and middle crust as well.

A chemical bias is also possible if the lower crust is systematically less alkaline than the upper crust from which we calibrate our

model. Such a bias would cause a higher estimate of heat production for the same seismic velocity. The result would be similar to the observations made with respect to oceanic and continental basalts and their log-linear models (Section 5.3.1). The average lower crustal model by Rudnick and Gao (2003) is in fact less alkaline than the high velocity upper crustal rocks. Their estimate for the lower crust, $\text{SiO}_2 = 53.4$ wt.% and $\text{Na}_2\text{O} + \text{K}_2\text{O} = 3.26$ wt.%, falls within the gabbroic diorite field. For the same SiO_2 content, the median alkali content of our model is 4.34 wt.% and mean 4.85 wt.%. Predicted MALI for the average lower crustal is -6.33 (Rudnick and Gao, 2003). The median heat production we would predict from this MALI is only slightly higher than estimated by Rudnick and Gao (2003).

While this may resolve the difference, it does not necessarily invalidate our model since the average lower crustal model may also be incorrect. Models of average crustal composition are carefully crafted from surficial chemistry, exhumed deep crustal sections, xenoliths, with adjustments for geophysical constraints provided by seismic models of the crust and surface heat flow (Rudnick and Gao, 2003). However, there are many assumptions that factor into these average continental models, which may be incorrect. For example, exhumed crustal sections and xenolith samples may not be representative of the lower crust, which is entirely possible given their rarity and poor spatial distribution. In addition, the surface heat flow constraint on average lower crustal composition is predicated on assumptions about lower crustal heat production and mantle heat flow that are difficult to constrain (Hasterok and Chapman, 2011; Hasterok and Gard, 2016).

Perhaps, the heat production–seismic velocity models from this and future studies can be used to improve estimates of continental crustal composition as well.

5.5. Additional caveats

5.5.1. Hydration related uncertainty

Hydration generally reduces the density and seismic velocity of igneous rocks with respect to an anhydrous composition (Hacker et al., 2003). Since hydrous compositions are not considered in the Behn and Kelemen (2003) empirical model of seismic velocity nor our estimates of density we must consider their impact on our estimated physical properties.

Before computing the influence of H_2O content, we need to know how much water is contained within igneous rocks. A little more than 10% of the data contain observations of structurally bound water H_2O^+ . The water content ranges from <0.01 wt.% to ~ 10 wt.% with a median value of 0.9 wt.% for plutonic rocks and 1.1 wt.% for volcanic rocks (Fig. 16a and c). The distributions are broader for volcanic rocks than for plutonics, but both appear skewed toward higher values. Average water content systematically decreases with SiO_2 for plutonic rocks and to a lesser extent for volcanic rocks (Fig. 16b and d). The data are sufficiently well correlated that a log-linear relationship between SiO_2 and H_2O^+ content can be established.

Despite the hydration observed at the surface, petrologic evidence suggests that the lower crust may be generally dry (Yardley and Valley, 1997). In these cases, the heat production–velocity relationship should be sufficient to estimate heat production. However, electrical conductivity models that suggest that the lower crust may contain significant quantities of water in some regions (Wannamaker, 2000).

To consider the effect of hydration on the heat production–velocity relationship, we produce several thermodynamic models using Perplex (Connolly, 2009) for an average felsic rock

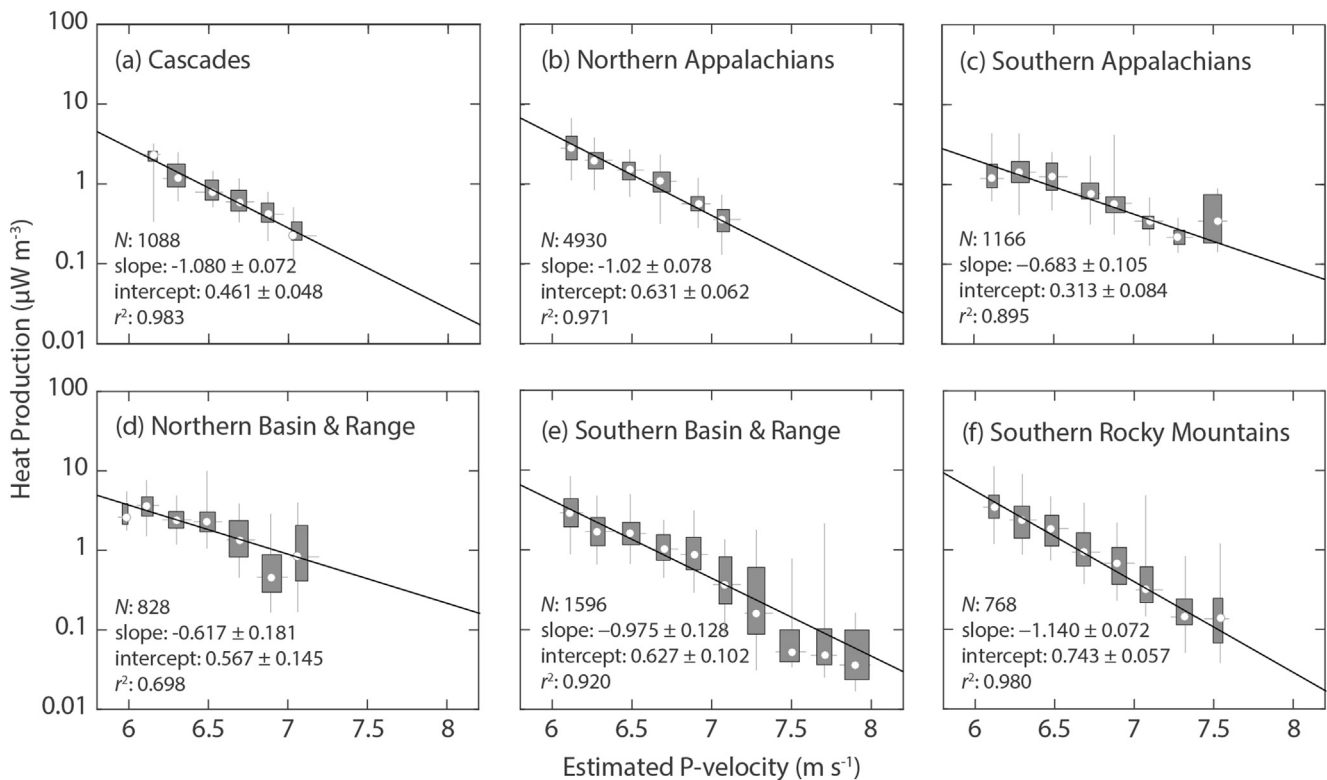


Figure 15. Heat production and estimated seismic velocity for plutonic rocks within North American geological provinces with ~ 1000 samples. The log-linear models are calibrated to median values between 6 and 7.4 km s^{-1} . Only velocity bins with greater than 10 points are shown.

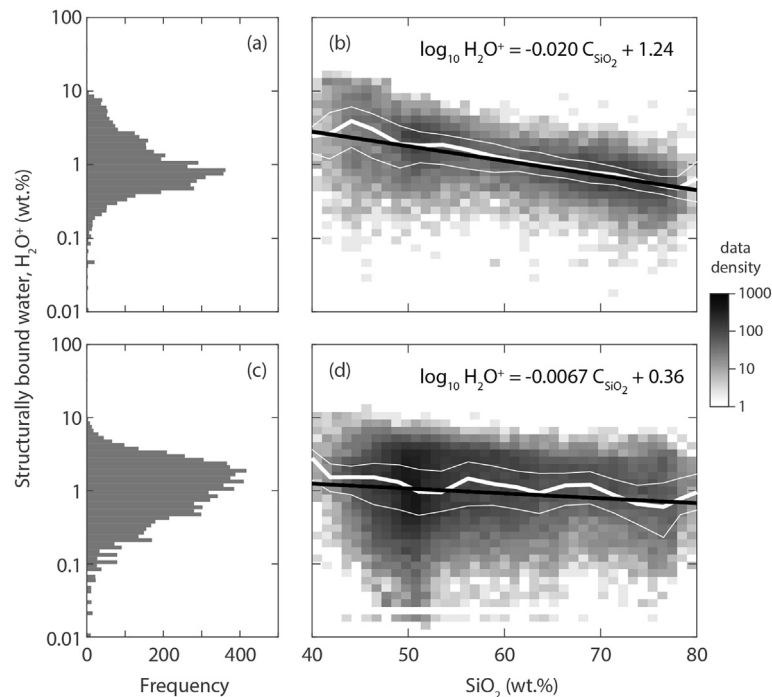


Figure 16. Structurally bound water content (H_2O^+) in igneous rocks. Distribution of H_2O^+ (a) and as a function of SiO_2 content (b) within plutonic rocks. (c, d) are similar plots for volcanic rocks. The lines in (b, d) represent the median (heavy white line) H_2O^+ content, 25% and 75% quantiles (light white lines) and log-linear fit to the data (black line).

($70 < C_{\text{SiO}_2} < 80$) and an average mafic rock ($52 < C_{\text{SiO}_2} < 57$) with water content varying from 0.01 to 10 wt.% (Table 1 in the [Supplementary Material](#)). Equilibrium phases, seismic velocity, and density are computed with the 2004 revised thermodynamic database (Holland and Powell, 1998; Connolly, 2009) and the equation of state by Pitzer and Sterner (1995).

Fig. 17 presents the summary of seismic velocity and density deviations from anhydrous conditions averaged between 0.5 and 2 GPa along an the three geotherms produced by Behn and Kelemen (2003). A more complete set of calculations is provided in the [Supplementary Material](#).

The average reduction in P-wave velocity under water-saturated conditions is $< 0.2 \text{ km s}^{-1}$ (2%) for an average granite and $< 0.7 \text{ km s}^{-1}$ (10%) for an average basalt (Fig. 17a and b). The effect of hydration is negligible at low water concentrations ($< 0.3 \text{ wt.}\%$) but increases until H_2O reaches saturation in the solid phase assemblage at which point the reduction is constant. Saturation is reached once H_2O exceeds $\sim 1.8 \text{ wt.}\%$ in granite (Fig. 17a) and $\sim 3 \text{ wt.}\%$ in basalt (Fig. 17b).

These computed saturation points are slightly higher than the estimates of median water content observed within this dataset for each respective rock type (Fig. 16). Therefore, we can expect the influence of hydration to be near the maximum reduction in velocity for about half of the samples. The reduction in velocity for granite is relatively small, falling within the anhydrous uncertainty bounds. Therefore, we can likely ignore this effect for felsic rocks. However, the reduction in seismic velocity on basalt will likely be sufficient to steepen the slope of heat production–velocity relationship for a hydrated crust. Note this cannot be the cause of the difference between the average heat production–velocity relationship and the average lower crust discussed in Section 5.4 because physical properties for both sets were computed under anhydrous conditions.

Results for density are more complex, with the potential for hydration to increase or decrease density with respect to the

anhydrous case along a geotherm. This results in a large standard deviation in the difference between hydrous and anhydrous conditions (Fig. 17c and d). For granite, the effect on density is generally small ($< 50 \text{ kg m}^{-3}$) and need not be considered (Fig. 17c). For basalt, the effect on density can be several hundred kg m^{-3} , but the magnitude and direction of the hydration effect are highly dependent upon the pressure and temperature for which the effect is considered (Fig. 17d). For example, the average effect on the density differences for the average and hot geotherms are less than those along the cold geotherm, which experiences a systematic decrease in density due to hydration in the basaltic case.

Since volumetric heat production depends on density (Eq. (1)), hydration will have an influence on heat production. However, given the complexity of the hydration effect on density it is perhaps best not applied to the heat production estimates since the physical state and composition must also be well known in order to apply an density accurate correction. In addition, the natural variability of heat production ranges over several orders of magnitude making the additional 10 to 20% uncertainty added by a hydration effect on density relatively small.

Generally the effect on velocity and density reduce estimates by no more than twice the uncertainty in anhydrous calculations. Because the reduction is on the order of a few percent maximum for any sample with many less than this amount, we do not expect the effect to prevent the use of our anhydrous model to produce reasonable estimates of crustal heat production. Because few data include H_2O^+ measurements ($\sim 10\%$ of the samples), it is not possible to assess the full impact on the database. Furthermore, a more extensive set of hydration models spanning the igneous compositions within the database are necessary given the complexity of the thermodynamic models. Such a modeling exercise is beyond the scope of this study and may be considered as part of a future study.

We must offer one additional word of caution when attempting to correct seismic velocity or heat production (via density). These

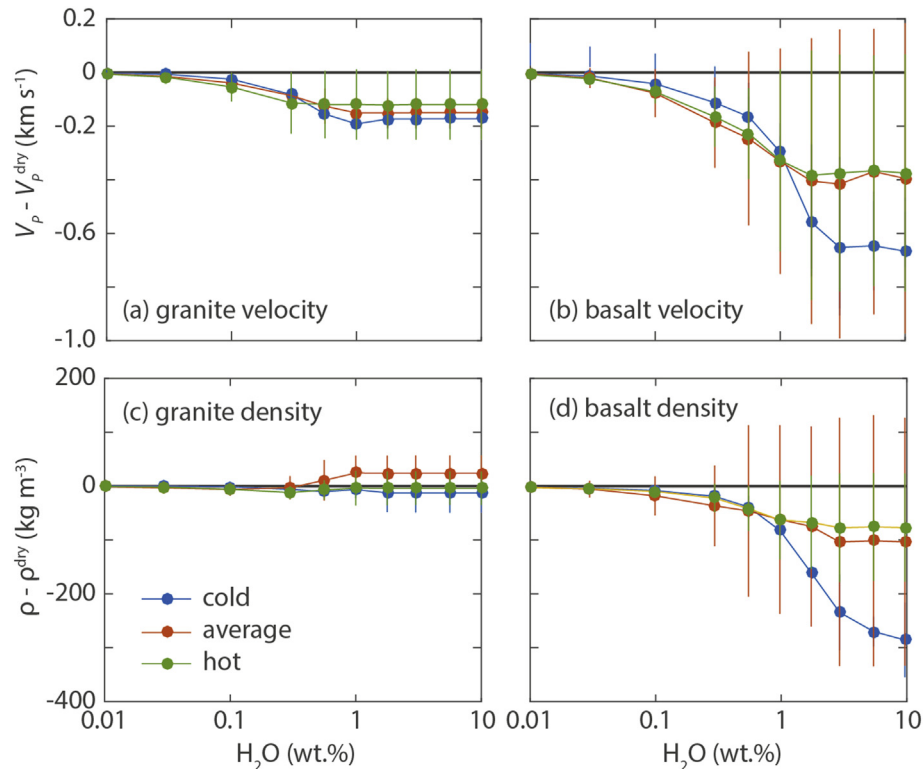


Figure 17. The influence of hydration on velocity (a, b) and density (c, d) for an average granitic (a, c) and basaltic (b, d) compositions. Thermodynamic models are averaged (points and connecting lines) along a cold (35 mW m^{-2}), average (56 mW m^{-2}) and hot geotherm (95 mW m^{-2}) from 0.5 to 2 GPa. The vertical bars represent the 2σ about the mean parameter estimates along the geotherm.

thermodynamic models assume equilibrium conditions, however, there are many instances where the mineral assemblages do not reach equilibrium or are metastable due to reaction kinetics (Hacker et al., 2005). Thus applying hydration corrections produced by equilibrium thermodynamic calculations like those presented here must be applied only when conditions near thermodynamic equilibrium can be assured.

5.5.2. Porosity

Porosity is typically of concern at depths shallower than ~ 10 km where even plutonic rocks can have significant porosity due to fractures. Deeper than 10 km, overlying pressure closes off nearly all void space (Christensen and Mooney, 1995). While hand samples of plutonic rocks tend to have porosity less than a few percent, the porosity of volcanic rocks can be significant ($>10\%$). It is possible to correct V_p estimates for porosity, but it must be tailored to the individual rock samples/units (Appendix A in Hasterok and Chapman, 2007). We could not adjust samples or our heat production models for porosity because porosity data are not reported within the geochemical databases.

6. Conclusions

Heat production is an uncertain physical property of the lithosphere because it is dependent upon trace element concentrations that do not directly affect geophysical quantities. One exception is surface heat flow, but it is difficult to separate the effects of internal heat generation (especially depth variations) from heat flow without additional constraints on mantle heat loss and/or lithospheric temperatures.

In this study, we develop a method for producing predictive empirical models of lithospheric heat production using seismic

velocity as a proxy. We show that despite large ranges in natural heat production, systematic trends in the average behavior are observed with variations in chemistry, specifically SiO_2 and total alkali content. Heat production tends to increase as both SiO_2 and total content increase. Additionally a significant relationship is observed between the modified alkali-lime index (MALI) and heat production. We find the heat production of volcanic rocks are generally similar to those of plutonic rocks.

These trends that occur within igneous rocks probably arise from the dominant process of differentiation through melting and crystallization. However, it is difficult to attribute the trends directly to a single physical process due to the complexities of source composition, evolution, and fluid alteration that affect each sample differently. While these correlations may not be directly causal, they can still be exploited to estimate average heat production from seismic velocity on a regional basis. These empirical relationships perform the best in the regions where subalkaline igneous rocks and places where S- and A-type igneous rocks dominate.

We do not suggest that a log-linear relationship between seismic velocity and heat production exists in all cases or for all rock types. Among igneous rocks, the relationship does not hold for extremely silica-rich rocks produced by precipitation of magmatic-derived hydrothermal fluids (silexites and quartzolites) and highly alkaline I-type igneous rocks, more specifically magnesian metaluminous alkalic and alkali-calcic compositions. However, both of these cases represent a very small fraction of the compositional distribution of igneous rocks but prevent the relationship from extending outside the calibrated velocity range (6.0 to 7.4 km s^{-1}). A log-linear relationship will also likely fail for shallow volcanic rocks with significant porosity and nearly all rocks shallower than ~ 5 to 10 km due to cracks which affect the propagation of seismic

waves. We also do not expect a log-linear relationship in local settings where the area and compositions of exposed rocks are insufficient to develop a reliable, representative relationship for the lithosphere below.

Average heat production of subalkaline mafic rocks are lower within the oceans than on the continents. Otherwise the heat production is similar for both domains. Heat production varies between continents, but has a similar slopes for log-linear heat production–seismic velocity relationships.

Average heat production is systematically higher within Australia than North America consistent with previous observations and heat flow studies. Robust linear relationships established for Finland (Fennoscandian Shield) and several geological provinces within North America support the use seismic velocities to estimate heat production vertically through the lithosphere on a regional basis.

The empirical estimation of heat production from seismic velocity provides valuable and reasonable constraints on the vertical distribution of heat production and its uncertainty, particularly in regions absent of other constraints. Use of a log-linear relationship is also preferable to the most commonly employed method used to estimate lithospheric heat production—guessing.

For continental regions, the average heat production of plutonic rocks can be estimated from the seismic velocity by

$$A = 3.80 \exp[-2.03(V_p - 6)] \quad (6)$$

where heat production, A , is in $\mu\text{W m}^{-3}$ and seismic P-wave velocity, V_p , is in km s^{-1} .

It remains an open question whether metamorphic and sedimentary rocks show similar behavior, which we intend to address in future studies. Future investigations will also focus on the applicability of these models to a greater range of regional settings and developing methods to verify the results using independent constraints.

Acknowledgements

DH would like to thank J. Foden for helpful discussions of igneous petrology, D. Kelsey for help running *Perple_X*, and M. Hand who gave helpful suggestions for improving the manuscript. D. Champion provided an prerelease version of the *OZChem* database. We would also like to thank the editor, M. Santosh and four anonymous reviewers for helpful comments that helped clarify our results. J. Webb was supported by a University of Adelaide summer research scholarship as part of this work.

Appendix A. Supplementary data

Supplementary data related to this article can be found at <http://dx.doi.org/10.1016/j.gsf.2017.03.006>.

References

- Abers, G., Hacker, B., 2016. A MATLAB toolbox and Excel workbook for calculating the densities, seismic wave speeds, and major element composition of minerals and rocks at pressure and temperature. *Geochemistry, Geophysics, Geosystems* 17, 616–624.
- Afonso, J., Fernández, M., Ranalli, G., Griffin, W., Connolly, J., 2008. Integrated geophysical–petrological modeling of the lithosphere and sublithospheric upper mantle: methodology and applications. *Geochemistry, Geophysics, Geosystems* 9, Q05008.
- Artemieva, I., 2006. Global $1^\circ \times 1^\circ$ thermal model *tc1* for the continental lithosphere: implications for lithosphere secular evolution. *Tectonophysics* 416, 245–277.
- Artemieva, I., Mooney, W., 2001. Thermal thickness and evolution of Precambrian lithosphere: a global study. *Journal of Geophysical Research* 106, 16387–16414.
- Bass, J., 1995. Elasticity of minerals, glasses, and melts. In: Ahrens, T. (Ed.), *A Handbook of Physical Constants: Mineral Physics and Crystallography*. Vol. 2 of AGU Ref. Shelf. AGU, Washington, D.C., pp. 45–63.
- Behn, M., Kelemen, P.B., 2003. Relationship between seismic p-wave velocity and the composition of anhydrous igneous and meta-igneous rocks. *Geochemistry, Geophysics, Geosystems* 4, 1041.
- Belousova, E., Griffin, W., O'Reilly, S.Y., Fisher, N., aug 2002. Igneous zircon: trace element composition as an indicator of source rock type. *Contributions to Mineralogy and Petrology* 143 (5), 602–622. <http://dx.doi.org/10.1007/s00410-002-0364-7>.
- Berryman, J., 1995. Mixture theories for rock properties. In: Ahrens, T. (Ed.), *A Handbook of Physical Constants: Rock Physics and Phase Relations*. Vol. 3 of AGU Ref. Shelf. AGU, Washington, D.C., pp. 205–228.
- Bonin, B., 2007. A-type granites and related rocks: evolution of a concept, problems and prospects. *Lithos* 97, 1–29.
- Brady, R., Ducea, M., Kidder, S., Saleeby, J., 2006. The distribution of radiogenic heat production as a function of depth in the Sierra Nevada Batholith, California. *Lithos* 86, 229–244.
- Brandle, J., Nagy, G., 1995. The state of the 5th version of the IGBA: igneous petrological data base. *Computers & Geosciences* 21, 425–432.
- Brown, M., 2014. The contribution of metamorphic petrology to understanding lithosphere evolution and geodynamics. *Geoscience Frontiers* 5 (4), 553–569. <http://dx.doi.org/10.1016/j.gsf.2014.02.005>.
- Champion, D., Budd, A., Hazell, M., Sedgmen, A., 2016. *Ozchem National Whole Rock Geochemistry Dataset*. Tech. Rep. Downloaded July 2016. Geoscience Australia.
- Chapman, D., Pollack, H., 1977. Regional geotherms and lithospheric thickness. *Geology* 5, 265–268.
- Chappell, B., White, A., 1992. I- and S-type granites in the Lachlan Fold Belt. *Transactions of the Royal Society of Edinburgh, Earth Sciences* 83, 1–26.
- Christensen, N., Mooney, W., 1995. Seismic velocity structure and composition of the continental crust: a global view. *Journal of Geophysical Research* 100, 9761–9788.
- Collins, W., Beams, S., White, A., Chappell, B., 1992. Nature and origin of A-type granites with particular reference to southeastern Australia. *Contributions to Mineralogy and Petrology* 80, 189–200.
- Connolly, J., 1990. Multivariable phase diagrams: an algorithm based on generalized thermodynamic. *American Journal of Science* 290, 666–718.
- Connolly, J.A.D., oct 2009. The geodynamic equation of state: what and how. *Geochemistry, Geophysics, Geosystems* 10 (10). <http://dx.doi.org/10.1029/2009GC002540>. n/a–n/a.
- Dawson, J., 1984. Contrasting types of mantle metasomatism? In: Kornprobst, J. (Ed.), *Kimberlites II: The Mantle and Crust-Mantle Relationships*. Elsevier, Amsterdam, pp. 289–294.
- Ernst, R., Buchan, K., 2010. *Geochemical database of Proterozoic intraplate mafic magmatism in Canada*. Open File 6016 6016. Geological Survey of Canada.
- Fountain, D., 1987. The relationship between seismic velocity and heat production—reply. *Earth and Planetary Science Letters* 83, 178–180.
- Frost, B., Barnes, C., Collins, W., Arculus, R., Ellis, D., Frost, C., 2001. A geochemical classification for granitic rocks. *Journal of Petrology* 42, 2033–2048. Geological Survey of Greenland, 2011. Ujarassiorit 1989–2011. Tech. rep. <http://www.ujarassiorit.gl>. Downloaded June 2016.
- Gerya, T.V., Maresch, W.V., Willner, A.P., Reenen, D.D.V., Smit, C., aug 2001. Inherent gravitational instability of thickened continental crust with regionally developed low- to medium-pressure granulite facies metamorphism. *Earth and Planetary Science Letters* 190 (3–4), 221–235. [http://dx.doi.org/10.1016/S0012-821X\(01\)00394-6](http://dx.doi.org/10.1016/S0012-821X(01)00394-6).
- Goes, S., van der Lee, S., 2002. Thermal structure of the North American uppermost mantle inferred from seismic tomography. *Journal of Geophysical Research* 107.
- Goldberg, K., Humayun, M., jul 2010. The applicability of the chemical index of alteration as a paleoclimatic indicator: an example from the permian of the paraná basin, Brazil. *Palaeogeography, Palaeoclimatology, Palaeoecology* 293 (1–2), 175–183. <http://dx.doi.org/10.1016/j.palaeo.2010.05.015>.
- Griffin, W., O'Reilly, S., Ryan, C., 1999. The composition and origin of subcontinental lithospheric mantle. In: Fei, Y., Bertka, C., Mysen, B. (Eds.), *Mantle Petrology: Field Observations and High Pressure Experimentation: A Tribute to Francis R. (Joe) Boyd*. Special Publication 6. Geochemical Society, St. Louis, MO, pp. 13–45.
- Hacker, B., Abers, G., Peacock, S., jan 2003. Subduction factory 1. Theoretical mineralogy, densities, seismic wave speeds, and H₂O contents. *Journal of Geophysical Research* 108 (B1), B12029. <http://dx.doi.org/10.1029/2001JB001127>.
- Hacker, B.R., Abers, G.A., Peacock, S.M., Johnston, S., feb 2005. Reply to comment by r. bousquet et al. on “subduction factory: 1. theoretical mineralogy, densities, seismic wave speeds and h₂o contents”. *Journal of Geophysical Research: Solid Earth* 110 (B2). <http://dx.doi.org/10.1029/2004JB003490>.
- Hasterok, D., Chapman, D., 2007. Continental thermal isostasy I: methods and sensitivity. *Journal of Geophysical Research* 112, B06414.
- Hasterok, D., Chapman, D., 2011. Heat production and geotherms for the continental lithosphere. *Earth and Planetary Science Letters* 307, 59–70.
- Hasterok, D., Gard, M., 2016. Utilizing thermal isostasy to estimate sub-lithospheric heat flow and anomalous crustal radioactivity. *Earth and Planetary Science Letters* 450, 197–207.
- Haus, M., Pauk, T., 2010. Data from the PETROCH lithogeochemical database. *Miscellaneous release—data 250*. Ontario Geological Survey.
- Holland, T., Powell, R., 1998. An internally consistent thermodynamic data set for phases of petrological interest. *Journal of Metamorphic Geology* 16, 309–343.
- Humphreys, E.R., Niu, Y., sep 2009. On the composition of ocean island basalts (OIB): the effects of lithospheric thickness variation and mantle metasomatism. *Lithos* 112 (1–2), 118–136. <http://dx.doi.org/10.1016/j.lithos.2009.04.038>.

- Jaupart, C., Mareschal, J.-C., 2003. Constraints on crustal heat production from heat flow data. In: Rudnick, R. (Ed.), *Treatise on Geochemistry: The Crust*, vol. 3. Elsevier, pp. 65–84. Ch. 2.
- Jaupart, C., Mareschal, J.-C., Iarotsky, L., 2016. Radiogenic heat production in the continental crust. *Lithos* 262, 398–427.
- Kelsey, D., Hand, M., 2015. On ultrahigh temperature crustal metamorphism: phase equilibria, trace element thermometry, bulk composition, heat sources, time-scales and tectonic settings. *Geoscience Frontiers* 6, 311–356.
- Kelsey, D.E., Clark, C., Hand, M., feb 2008. Thermobarometric modelling of zircon and monazite growth in melt-bearing systems: examples using model metapelitic and metapsammitic granulites. *Journal of Metamorphic Geology* 26 (2), 199–212. <http://dx.doi.org/10.1111/j.1525-1314.2007.00757.x>.
- Kramers, J., Kreissig, K., Jones, M., 2001. Crustal heat production and style of metamorphism: a comparison between two Archean high grade provinces in the Limpopo Belt, southern Africa. *Precambrian Research* 112, 149–163.
- Le Bas, M., Streckeisen, A., 1991. The iugs systematics of igneous rocks. *Journal of the Geological Society London* 148, 825–833.
- Lett, R., Ronning, C., 2005. The BC rock geochemical database. *Geofile* 2005-14. Geological Survey of British Columbia.
- McKenzie, D., Jackson, J., Priestley, K., 2005. Thermal structure of oceanic and continental lithosphere. *Earth and Planetary Science Letters* 233, 337–349.
- McLaren, S., Sandiford, M., Hand, M., 1999. High radiogenic heat-producing granites and metamorphism—an example from the Mt. Isa inlier, Australia. *Geology* 27, 679–682.
- McLaren, S., Sandiford, M., Hand, M., Neumann, N., Wyborn, L., Bastrakova, I., 2003. The Hot South Continent: Heat Flow and Heat Production in Australian Proterozoic Terranes. Vol. 22 of Special Pub. Geological Society of Australia, pp. 151–161.
- Middlemost, E., 1994. Naming materials in the magma/igneous rock system. *Earth-Science Reviews* 37, 215–224.
- Neumann, N., Sandiford, M., Foden, J., 2000. Regional geochemistry and continental heat flow: implications for the origin of the South Australian heat flow anomaly. *Earth and Planetary Science Letters* 183, 107–120.
- Newfoundland and Labrador Geological Survey, 2009a. Plutonic Database. Newfoundland and Labrador GeoScience Atlas OnLine. Last update: September 2010. <http://geoatlas.gov.nl.ca>. Downloaded June 2016. Tech. rep.
- Newfoundland and Labrador Geological Survey, 2009b. Volcanic Database. Newfoundland and Labrador GeoScience Atlas OnLine. Last update: August 2009. <http://geoatlas.gov.nl.ca>. Downloaded June 2016. Tech. rep.
- Philpotts, A., Ague, J., 2009. *Principles of Igneous and Metamorphic Petrology*, second ed. Cambridge.
- Pitzer, K.S., Sterner, S.M., mar 1995. Equations of state valid continuously from zero to extreme pressures with H₂O and CO₂ as examples. *International Journal of Thermophysics* 16 (2), 511–518. <http://dx.doi.org/10.1007/BF01441917>.
- Rasilainen, K., Lahtinen, R., Bomhorst, T., 2007. *The Rock Geochemical Database of Finland Manual*. (Online). Report of Investigation 164, Geological Survey of Finland.
- Roy, S., Ray, L., Bhattacharya, A., Srinivasan, R., 2008. Heat flow and crustal thermal structure in the Late Archean Clospet granite batholith, south India. *International Journal of Earth Sciences* 97, 245–256.
- Rudnick, R., Gao, S., 2003. Composition of the continental crust. In: Rudnick, R. (Ed.), *Treatise on Geochemistry: The Crust*, vol. 3. Elsevier, pp. 1–64. Ch. 1.
- Rudnick, R., McDonough, W., O'Connell, R., 1998. Thermal structure, thickness and composition of continental lithosphere. *Chemical Geology* 145, 395–411.
- Rybach, L., 1973. Radioactive heat production of rocks from the Swiss alps: geophysical implications. In: 1st European Geophysical Society Meeting, Zurich.
- Rybach, L., 1978/79. The relationship between seismic velocity and radioactive heat production in continental rocks. *Pageoph* 117, 75–82.
- Rybach, L., 1988. Determination of heat production rate. In: Hänel, R., Rybach, L., Stegena, I. (Eds.), *Terrestrial Handbook of Heat-flow Density Determination*. Kluwer Academic Publishers, Dordrecht, pp. 125–142. Ch. 4.2.
- Rybach, L., Buntebarth, G., 1982. Relationships between the petrophysical properties density, seismic velocity, heat generation, and mineralogical constitution. *Earth and Planetary Science Letters* 57, 367–376.
- Rybach, L., Buntebarth, G., 1984. The variation of heat generation, density and seismic velocity with rock type in the continental lithosphere. *Tectonophysics* 103, 335–344.
- Sandiford, M., Hand, M., McLaren, S., 2001. Tectonic feedback, intraplate orogeny and the geochemical structure of the crust: a central Australian perspective. In: Miller, J., Holdsworth, J., Buick, L., Hand, M. (Eds.), *Continental Reactivation and Reworking*. Vol. 184 of Special Publication of Geological Society London, pp. 195–218.
- Sobolev, S., Babeyko, A., 1994. Modeling of mineralogical composition, density and elastic wave velocities in anhydrous magmatic rocks. *Surveys in Geophysics* 15, 515–544.
- Stixrude, L., Lithgow-Bertelloni, C., 2005. Thermodynamics of mantle minerals – I. physical properties. *Geophysical Journal International* 162, 610–632.
- Strong, D., Turnbull, R., Haubrock, S., Mortimer, N., 2016. Petlab: New Zealand's national rock catalogue and geoanalytical database. *New Zealand Journal of Geology and Geophysics* 59.
- Telford, W., Goldart, L., Sheriff, R., 1990. *Applied Geophysics*, second ed. Cambridge Univ. Press.
- Wannamaker, P., 2000. Comment on “the petrologic case for a dry lower crust” by b.w.d. yardley and j.w. valley. *Journal of Geophysical Research* 105, 6057–6064.
- Whalen, J., Sanborn-Barrie, M., Young, M., 2012. Geochemical data from Archean and Paleoproterozoic plutonic and volcanic rocks of Cumberland Peninsula, eastern Baffin island, Nunavut. Open file 6933. Geological Survey of Canada.
- Yardley, B., Valley, J., 1997. The petrologic case for a dry lower crust. *Journal of Geophysical Research* 102, 12173–12185.
- Zunino, A., Connolly, J.A.D., Khan, A., apr 2011. Precalculated phase equilibrium models for geophysical properties of the crust and mantle as a function of composition. *Geochemistry, Geophysics, Geosystems* 12 (4). <http://dx.doi.org/10.1029/2010GC003304>. n/a–n/a.